
PROVABLY ROBUST BAYESIAN COUNTERFACTUAL EXPLANATIONS UNDER MODEL CHANGES

Jamie Duell

School of Computing and Digital Technologies
Sheffield Hallam University
j.duell@shu.ac.uk

Xiuyi Fan

Lee Kong Chian School of Medicine
Nanyang Technological University
xyfan@ntu.edu.sg

February 12, 2026

ABSTRACT

Counterfactual explanations (CEs) offer interpretable insights into machine learning predictions by answering “what if?” questions. However, in real-world settings where models are frequently updated, existing counterfactual explanations can quickly become invalid or unreliable. In this paper, we introduce Probabilistically Safe CEs (PSCE), a method for generating counterfactual explanations that are δ -safe, to ensure high predictive confidence, and ϵ -robust to ensure low predictive variance. Based on Bayesian principles, PSCE provides formal probabilistic guarantees for CEs under model changes which are adhered to in what we refer to as the $\langle \delta, \epsilon \rangle$ -set. Uncertainty-aware constraints are integrated into our optimization framework and we validate our method empirically across diverse datasets. We compare our approach against state-of-the-art Bayesian CE methods, where PSCE produces counterfactual explanations that are not only more plausible and discriminative, but also provably robust under model change.

1 Introduction

Counterfactual Explanations (CEs) have gained traction as a way to answer “what-if?” questions in machine learning (ML) (Wachter et al., 2018). A CE typically seeks a minimal alteration to an input that changes the model’s prediction to a desired class. To be reliable, CEs should satisfy core desiderata such as *proximity*, *validity*, *discriminativeness*, *robustness* and *plausibility* (Sokol and Hüllermeier, 2025). However, a critical challenge often overlooked is the robustness of CEs in dynamic environments. When an underlying ML model is updated, which is a common scenario in real-world applications such as online and continual learning (Hoi et al., 2018; van de Ven et al., 2022) explanations, the generated for the original model may become invalid. Small shifts in model parameters can move decision boundaries, rendering previous CEs useless.

While some recent work has proposed post-hoc methods to update CEs after a model changes (Hamman et al., 2023; Stepka et al., 2025), a more principled approach is to generate explanations that are inherently robust to such perturbations from the outset. This requires integrating model uncertainty directly into the CE generation process. By considering a distribution over model parameters, as is natural in Bayesian frameworks like Bayesian Neural Networks (BNNs) (Tran et al., 2019) or Monte Carlo Dropout (MC Dropout) (Gal and Ghahramani, 2016), we can search for CEs that are not just valid for a single point estimate of the model, but remain valid across a whole family of plausible models.

The core intuition is that a robust CE should be classified with both 1) high predictive certainty (a high mean probability for the target class) and 2) low predictive variance across the model posterior. A CE with these properties resides deep within the target class’s decision region, creating a “safety buffer” that makes it resilient to minor shifts in the decision boundary caused by model changes. To formalize this, we introduce Probabilistically Safe Counterfactual Explanations (PSCE), a Bayesian-inspired method that generates CEs with formal guarantees on their robustness. PSCE optimizes for counterfactuals that are not only robust but also plausible by encouraging them to lie on the data manifold. This results in coherent and interpretable outputs, as illustrated in the medical imaging example in Figure 1.

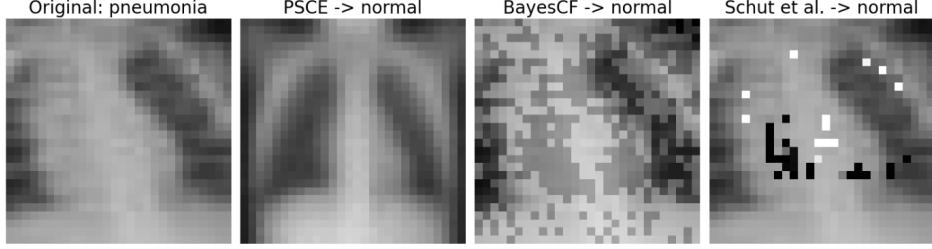


Figure 1: Counterfactual examples for a PneumoniaMNIST (Yang et al., 2021, 2023) image, transitioning from ‘pneumonia’(on the left) to ‘normal’. The output from our proposed method, PSCE, is shown alongside other Bayesian approaches discussed in this work.

Beyond generating plausible explanations, PSCE’s primary guarantee is robustness to model changes. We illustrate this core property with a simple example:

Example 1. Suppose a counterfactual is generated for a model trained on 70% of the available data. The model is then updated by training on an additional 5% of the data, causing its posterior distribution to shift. As shown in Figure 2, the predictive probability for the PSCE-generated counterfactual remains well above the required threshold, demonstrating its robustness to the model change. Our theoretical bound, introduced later, formally guarantees this outcome.

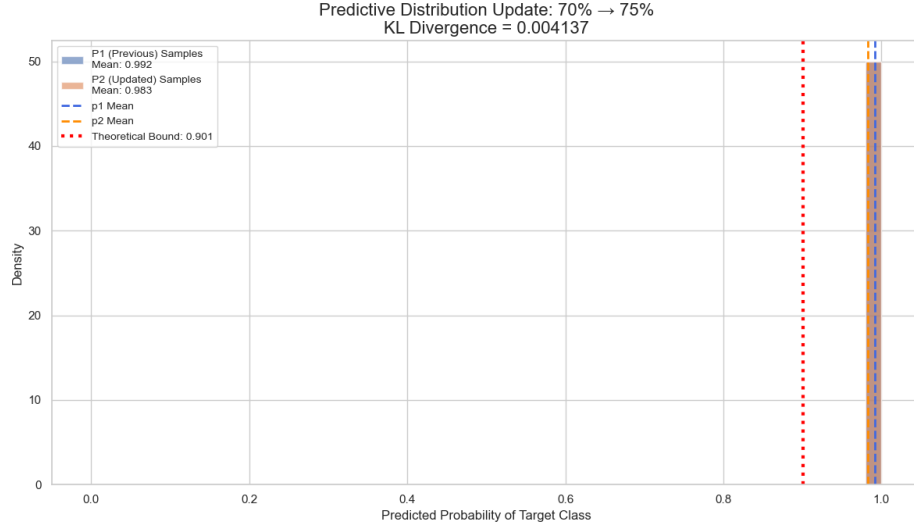


Figure 2: Predictive distribution for a CE before (p1) and after (p2) a 5% data increment. The PSCE-generated CE remains confidently classified, and the new prediction is well-described by our theoretical lower bound.

In this work, we compare PSCE against other Bayesian, model-specific CE methods: BayesCF (Batten et al., 2025) and Schut et al. (Schut et al., 2021). Our central contributions are threefold:

1. We introduce PSCE, a method for generating probabilistically safe counterfactuals that explicitly optimizes for high confidence and low variance.
2. We derive a theoretical bound that formally guarantees the validity of a counterfactual under a given magnitude of model change.
3. We empirically validate the robustness of PSCE against existing Bayesian CE methods, demonstrating its superior performance across key metrics from counterfactual literature.

2 Counterfactual Desiderata

In this section, we informally discuss counterfactual desiderata as per recent literature (Sokol and Hüllermeier, 2025), ensuring that our approach is principled. Thus, we have the following:

- **Validity:** Ensures the counterfactual instance falls into a desired counterfactual class.
- **Robustness:** Ensures that sufficiently small model changes do not invalidate counterfactual instances from being classified under the desired counterfactual class.
- **Plausibility:** Ensures that counterfactual instance is on the data manifold and thus is plausible as per the data.
- **Discriminativeness:** Ensures that the counterfactual is distinguishable, thus looks like it belongs to the counterfactual class.
- **Proximity:** Ensures that minimal changes are needed across all features to obtain a desired counterfactual instance.

3 Robust and Probabilistically Safe Counterfactuals

To begin with the building blocks that constitute the central objective function, we consider a Bayesian lens for classification, in which the model parameters ω are treated as random variables with a posterior distribution given the data \mathcal{D} . This takes the form:

$$p(\omega|\mathcal{D}) = \frac{p(\mathcal{D}|\omega)p(\omega)}{p(\mathcal{D})},$$

where $p(\omega|\mathcal{D})$ is the posterior distribution of the model parameters given the training data \mathcal{D} . In this work, we use both BNNs (Tran et al., 2019) and MC Dropout (Gal and Ghahramani, 2016) to approximate $p(\omega|\mathcal{D})$. From a Bayesian perspective, we begin by defining a classifier:

Definition 1 (Bayesian Classifier). *A classifier with parameters ω maps an input $\mathbf{x} \in \mathbf{X}$ to logits:*

$$\mathbf{l}(\mathbf{x}; \omega) = \langle l_1(\mathbf{x}; \omega), \dots, l_C(\mathbf{x}; \omega) \rangle \in \mathbb{R}^C,$$

the class probabilities are obtained via the softmax transformation:

$$f_c(\mathbf{x}; \omega) = \frac{\exp(l_c(\mathbf{x}; \omega))}{\sum_{i=1}^C \exp(l_i(\mathbf{x}; \omega))}, \quad c = 1, \dots, C.$$

Under the Bayesian formulation, the posterior predictive distribution is given by:

$$p(y = c|\mathbf{x}, \mathcal{D}) = \mathbb{E}_{\omega \sim p(\omega|\mathcal{D})} \left[f_c(\mathbf{x}; \omega) \right],$$

the predicted label is:

$$y = \arg \max_{c \in \{1, \dots, C\}} p(y = c|\mathbf{x}, \mathcal{D}).$$

Given a classifier, we can then define a counterfactual instance from a Bayesian perspective to be given:

Definition 2 (Counterfactual Instance). *Let $\mathbf{x} \in \mathbb{R}^J$ be an instance, $\mathcal{G}_{CF} : \mathbb{R}^J \rightarrow \mathbb{R}^J$ a counterfactual generator, and y the predicted class of \mathbf{x} under the Bayesian classifier. A counterfactual instance \mathbf{x}' produced by a counterfactual generator \mathcal{G}_{CF} satisfies:*

$$\begin{aligned} \mathbf{x}' : \arg \max_{c \in \{1, \dots, C\}} p(y' = c|\mathbf{x}', \mathcal{D}) &\neq y \\ \text{where, } \mathbf{x}' &= \mathcal{G}_{CF}(\mathbf{x}). \end{aligned}$$

where, y' is the counterfactual class.

A posterior predictive distribution for a counterfactual \mathbf{x}' belonging to a counterfactual class y' is given as:

$$p(y'|\mathbf{x}', \mathcal{D}) = \int p(y'|\mathbf{x}', \omega)p(\omega|\mathcal{D})d\omega = \mathbb{E}_{\omega \sim p(\omega|\mathcal{D})} \left[p(y'|\mathbf{x}', \omega) \right].$$

To ensure counterfactuals remain valid, we additionally require that they lie in high-likelihood regions of the data distribution, which we model via a generative density $p_\theta(\mathbf{x})$ in the model. The likelihood of a candidate counterfactual instance \mathbf{x}' being valid can be assessed through the learned likelihood $p_\theta(\mathbf{x})$. Parameters θ are optimised for the dataset \mathbf{X} according to:

$$\theta^* := \arg \max_{\theta} \frac{1}{|\mathbf{X}|} \sum_{\mathbf{x} \in \mathbf{X}} \log p_\theta(\mathbf{x}) = \arg \max_{\theta} \frac{1}{|\mathbf{X}|} \sum_{\mathbf{x} \in \mathbf{X}} \log \int p_\theta(\mathbf{x}|\mathbf{z})p(\mathbf{z})d\mathbf{z}.$$

This corresponds to maximising the marginal log-likelihood of the data. In doing so, p_θ approximates the true data distribution \mathcal{D} , such that any new counterfactual instance $\mathbf{x}' \sim \mathcal{D}$ is expected to have high likelihood under the distribution p_θ .

As suggested, a common occurrence in real-world deployment is *model change*. Existing works discuss robustness to model change (Jiang et al., 2024), which informally states that a counterfactual remains valid under a “sufficiently small” change in model parameters. Our strategy, is to propose a tractable optimization scheme to quantify robustness under model changes. The intuition is that a counterfactual instance which is confidently embedded within the target class’s decision region for some original model is more likely to survive minor shifts in the decision boundary from a model change, this sentiment is shared in the work (Hamman et al., 2023). We can formalize this by ensuring that two properties affiliated with the posterior $p(\omega|\mathcal{D})$ are encouraged, namely:

- High Predictive Certainty: The model should, on average, classify the counterfactual with very high confidence.
- Low Predictive Variance: The prediction should be stable across all plausible versions of the model described by the posterior. High variance would imply that some versions of the model already place the counterfactual near or over a decision boundary, thus making it fragile.

These two properties give rise to our building blocks: δ -safety and ϵ -robustness. We later provide a theoretical bound on the robustness and safety of a counterfactual under model changes under an updated posterior which cannot be known before hand.

To begin, we say a counterfactual is δ -safe, if the posterior predictive distribution falls safely over a decision threshold $1 - \delta$ for $\delta \in [0, 1]$. More formally:

Definition 3 (δ -safe Counterfactual). *Given a counterfactual class y' and a data distribution \mathcal{D} , a counterfactual \mathbf{x}' is considered δ -safe, if and only if:*

$$p(y'|\mathbf{x}', \mathcal{D}) \geq 1 - \delta.$$

Extending this, we consider a counterfactual to be ϵ -robust, if the variance of the likelihood falls under some threshold ϵ . Formally,

Definition 4 (ϵ -robust Counterfactual). *Given a counterfactual class y' , a data distribution \mathcal{D} and a distribution defined over model weights given the data distribution $p(\omega|\mathcal{D})$, we consider a counterfactual \mathbf{x}' to be a ϵ -robust if and only if:*

$$\text{Var}_{\omega \sim p(\omega|\mathcal{D})} \left[p(y'|\mathbf{x}', \omega) \right] \leq \epsilon.$$

We take the approach, as this represents epistemic uncertainty which is reducible by definition, and thus optimizing variance under some threshold ϵ is a plausible approach to reduce uncertainty for a counterfactual instance \mathbf{x}' .

Finally, we can then prescribe rules for what we name the $\langle \delta, \epsilon \rangle$ -set of counterfactual instances.

Definition 5 ($\langle \delta, \epsilon \rangle$ -Set). *Counterfactual instances \mathbf{x}' belong to the $\langle \delta, \epsilon \rangle$ -set ($S_{\langle \delta, \epsilon \rangle}$), where:*

$$S_{\langle \delta, \epsilon \rangle} := \{ \mathbf{x}' : p(y'|\mathbf{x}', \mathcal{D}) \geq 1 - \delta \wedge \text{Var}_{\omega \sim p(\omega|\mathcal{D})} \left[p(y'|\mathbf{x}', \omega) \right] \leq \epsilon \},$$

where the counterfactual instance \mathbf{x}' is both δ -safe, ϵ -robust.

The definition for the $\langle \delta, \epsilon \rangle$ -set, namely $S_{\langle \delta, \epsilon \rangle}$ ensures safety guarantees that consider both the standard deviation and the posterior predictive distribution. By filtering a set of counterfactual instances $S_{\langle \delta, \epsilon \rangle}$, we can ensure robustness to model changes, where we provide provable theoretical guarantees introduced in our central theorems, namely Theorem 1 and Theorem 2. We then proceed to empirically verify the utility of our central theorems.

4 Generating Counterfactuals

To achieve this, we ensure that a counterfactual is δ -safe, ϵ -robust and adheres to desiderata presented in the previous section. To this end, we propose the following optimization function to generate a robust counterfactual \mathbf{x}' , initialized at \mathbf{x} :

$$\mathbf{x}' := \mathcal{G}_{PSCE}(\mathbf{x}) = \arg \min_{\mathbf{x}'} (\lambda_1 \mathcal{L}_{clf} + \lambda_2 \mathcal{L}_{del} + \lambda_3 \mathcal{L}_{ldist} + \lambda_4 \mathcal{L}_{var} - \lambda_5 \mathcal{L}_{ELBO}).$$

From this optimization problem, we define each part independently. Thus, we have:

$$\mathcal{L}_{clf}(\mathbf{x}') = -\mathbb{E}_{\omega \sim p(\omega|\mathcal{D})}[\log p(y'|\mathbf{x}', \omega)].$$

The \mathcal{L}_{clf} term aims to ensure that the generated counterfactual \mathbf{x}' belongs to a counterfactual class y' , which corresponds to the negative expected log-likelihood over the posterior distribution of weights ω . We then introduce:

$$\mathcal{L}_{del}(\mathbf{x}') = \max((1 - \delta) - \mathbb{E}_{\omega \sim p(\omega|\mathcal{D})}[p(y'|\mathbf{x}', \omega)], 0),$$

which enforces that the predictive probability for \mathbf{x}' is at least $1 - \delta$, consistent with the definition of a δ -safe counterfactual. Under similar notation, we have the loss function aligning with an ϵ -robust counterfactual, given by:

$$\mathcal{L}_{var}(\mathbf{x}') = \max(\text{Var}_{\omega \sim p(\omega|\mathcal{D})}[p(y'|\mathbf{x}', \omega)] - \epsilon, 0).$$

Next, we consider plausibility. In the context of our work, plausibility refers to the likelihood of observing a counterfactual \mathbf{x}' under the data distribution \mathcal{D} , parameterized by θ' . In practice, one does not know the true distribution θ' , and thus optimization over some parameter θ to obtain an optimal θ^* such that $\theta' \approx \theta^*$ is computed. Thus, by equation 1, we follow the standard Variational Autoencoder (VAE) (Kingma and Welling, 2014) formulation, introducing the approximate posterior $q_\phi(\mathbf{z}|\mathbf{x})$ such that:

$$\log p(\mathbf{x}) = \log \int q_\phi(\mathbf{z}|\mathbf{x}) \frac{p_\theta(\mathbf{x}|\mathbf{z})p(\mathbf{z})}{q_\phi(\mathbf{z}|\mathbf{x})} d\mathbf{z}. \quad (1)$$

Assuming parameters $\{\theta^*, \phi^*\}$ are learned for the pretrained model. Then, we can adopt the standard Evidence Lower Bounds (ELBO) to ensure that a counterfactual \mathbf{x}' remains within the data distribution.

$$\mathcal{L}_{ELBO}(\mathbf{x}') = \mathbb{E}_{q_{\phi^*}(\mathbf{z}|\mathbf{x}')}[\log p_{\theta^*}(\mathbf{x}'|\mathbf{z})] + \mathbb{E}_{q_{\phi^*}(\mathbf{z}|\mathbf{x}')}[\log p(\mathbf{z})] - \mathbb{E}_{q_{\phi^*}(\mathbf{z}|\mathbf{x}')}[\log q_{\phi^*}(\mathbf{z}|\mathbf{x}')],$$

where θ^* and ϕ^* are given by a pretrained variational autoencoder (VAE), the standard ELBO derivation is provided in the *supplementary material*. All the expectations in this section are approximated through Monte Carlo sampling with dropout enabled at the time of inference or sampling over BNN weights.

To account for proximity, we adopt the technique of minimizing distance of generated samples within a latent space. Thus, given an instance \mathbf{x} and its counterfactual \mathbf{x}' , let $\mu_{\phi^*}(\mathbf{x})$ represent the mean encoded representation of \mathbf{x} , and $\mu_{\phi^*}(\mathbf{x}')$ be the mean encoded representation of \mathbf{x}' , then the final term of our objective function is given as:

$$\mathcal{L}_{ldist}(\mathbf{x}', \mathbf{x}) = \|\mu_{\phi^*}(\mathbf{x}) - \mu_{\phi^*}(\mathbf{x}')\|_2^2.$$

Informally, this encourages the encoded counterfactual to remain close to the encoded representation of the original instance. In principle, our approach provides optimization in accordance to the following desiderata:

- \mathcal{L}_{clf} ensures *validity* of the counterfactual, whereby \mathcal{L}_{del} ensures the *validity* is safe under a distribution of parameters $p(\omega|\mathcal{D})$ – which further inclines the safety of counterfactual explanations under model changes which we address in the next section (concerning *robustness*).
- \mathcal{L}_{var} ensures that the counterfactual is *validity* by encouraging epistemic uncertainty in counterfactual generation to be less than or equal to some ϵ .
- \mathcal{L}_{ELBO} and \mathcal{L}_{ldist} aim to ensure that 1) the counterfactual pathway is optimised such that it remains within the data distribution, encouraging *plausibility* and *discriminativeness*, while 2) being in close *proximity* to the origin.

More broadly, \mathcal{L}_{del} and \mathcal{L}_{var} focus on the certainty of a counterfactual instance, \mathcal{L}_{ELBO} ensures that the counterfactual is plausible under the learned data distribution, \mathcal{L}_{ldist} encourages similarity, and \mathcal{L}_{clf} directly guides the counterfactual towards the desired counterfactual class.

5 Counterfactual Robustness under model changes

In this section, we present Theorem 1 and 2, where the implication is that any counterfactual in the set $S_{\langle\delta,\epsilon\rangle}$ which is encouraged by PSCE has theoretical guarantees on the safety and robustness of a counterfactual instance under model changes. Thus, the theoretical analysis in this section follows assumption 1.

Assumption 1. *Counterfactual instances \mathbf{x}' belong to $S_{\langle\delta,\epsilon\rangle}$, the $\langle\delta,\epsilon\rangle$ -set.*

We first look at the safety of counterfactual instances under model changes, we begin by considering a single update to model parameters from some original data \mathcal{D}_{prev} and some new data \mathcal{D}_{new} , whereby a predictive posterior is given as:

$$p(y'|\mathbf{x}', \mathcal{D}_{prev}) = \int p(y'|\mathbf{x}', \omega) \cdot p_1(\omega|\mathcal{D}_{prev}) d\omega = \mathbb{E}_{\omega \sim p_1(\omega|\mathcal{D}_{prev})} [p(y'|\mathbf{x}', \omega)],$$

under the original model \mathcal{D}_{prev} , and the predictive posterior distribution of the new model is defined as:

$$p(y'|\mathbf{x}', \mathcal{D}_{prev} \cup \mathcal{D}_{new}) = \int p(y'|\mathbf{x}', \omega) \cdot p_2(\omega|\mathcal{D}_{prev} \cup \mathcal{D}_{new}) d\omega = \mathbb{E}_{\omega \sim p_2(\omega|\mathcal{D}_{prev} \cup \mathcal{D}_{new})} [p(y'|\mathbf{x}', \omega)].$$

Here, the posterior predictive distribution is eligible to change as a consequence of a change in the posterior distribution $p(\omega|\cdot)$. In which we consider a distribution over the previous data \mathcal{D}_{prev} and the distribution over new data \mathcal{D}_{new} , we can then prescribe a posterior distribution over model parameters under the old data (via. $p_1(\omega|\cdot)$), and new data (via $p_2(\omega|\cdot)$), giving

$$p_1(\omega|\mathcal{D}_{prev}) = \frac{p(\mathcal{D}_{prev}|\omega)p(\omega)}{p(\mathcal{D}_{prev})},$$

and

$$p_2(\omega|\mathcal{D}_{prev} \cup \mathcal{D}_{new}) = \frac{p(\mathcal{D}_{prev} \cup \mathcal{D}_{new}|\omega)p(\omega)}{p(\mathcal{D}_{prev} \cup \mathcal{D}_{new})}.$$

Assuming that model changes produce small change providing a new posterior distribution $p_2(\omega|\mathcal{D}_{prev} \cup \mathcal{D}_{new})$, that is, the Kullback-Leibler divergence between the old and new posterior is “sufficiently small” (Jiang et al., 2024) $D_{KL}(p_2(\omega|\cdot)||p_1(\omega|\cdot))$ (we explore this in the results section and the *supplementary material*). Theorem 1 illustrates a tight lower bound for the change in probability for a counterfactual instance \mathbf{x}' under the newly defined posterior distribution.

Table 1: Empirical example for the theoretical bound. A valid counterfactual \mathbf{x}' is selected such that $p_1(y'|\mathbf{x}', \mathcal{D}_{prev}) \geq 1 - \delta$, with $\delta = 0.05$ and a learning rate of $1e - 5$. The example uses the Wisconsin Breast Cancer dataset with a Bayesian Neural Network (BNN) to approximate $p_2(\omega|\cdot)$ and $p_1(\omega|\cdot)$.

Update	$p_1(y' \mathbf{x}')$	$p_2(y' \mathbf{x}')$	$\sim D_{KL}(p_2(\omega \cdot) p_1(\omega \cdot))$	Bound	Holds
95% → 96%	0.9977	0.9981	0.000330	0.9720	✓
96% → 97%	0.9981	0.9971	0.000355	0.9714	✓
97% → 98%	0.9971	0.9976	0.000096	0.9832	✓
98% → 99%	0.9976	0.9998	0.000423	0.9685	✓
99% → 100%	0.9998	0.9974	0.000477	0.9689	✓

Theorem 1. Let $p_1(\omega|\mathcal{D}_{prev})$ be a probabilistic model’s posterior distribution over its parameters ω . After a data update $\mathcal{D}_{prev} \cup \mathcal{D}_{new}$, the new posterior is $p_2(\omega|\mathcal{D}_{prev} \cup \mathcal{D}_{new})$. Given the initial posterior predictive probability for a class y' given a counterfactual \mathbf{x}' is at least $p_1(y'|\mathbf{x}', \mathcal{D}_{prev}) \geq 1 - \delta$, then the updated posterior predictive probability is bounded as:

$$\begin{aligned} & p_2(y'|\mathbf{x}', \mathcal{D}_{prev} \cup \mathcal{D}_{new}) \\ & \geq (1 - \delta) - 2 \cdot \sqrt{\frac{1}{2} D_{KL}(p_2(\omega|\cdot)||p_1(\omega|\cdot))}, \end{aligned}$$

where, $p_2(\omega|\cdot) = p_2(\omega|\mathcal{D}_{prev} \cup \mathcal{D}_{new})$ and $p_1(\omega|\cdot) = p_1(\omega|\mathcal{D}_{prev})$.

Thus, we have established that the predictive confidence degrades gracefully under model changes at a rate of $2 \cdot \sqrt{\frac{1}{2} D_{KL}(p_2(\omega|\cdot)||p_1(\omega|\cdot))}$ relative to the original threshold $1 - \delta$. Thus, a tighter update in the posterior distribution of model parameters under new data \mathcal{D}_{new} , the tighter the bound for a counterfactual under model changes. Consequently, we can plug in values directly and solve for D_{KL} , for example, we can consider a scenario where we have a δ -safe (for $\delta = 0.05$) counterfactual, and we wish that counterfactual stays above 50% probability towards a desired class, then as per Section C of the *supplementary material*, we have:

$$D_{KL}(p_2(\omega|\cdot)||p_1(\omega|\cdot)) \leq 0.10125,$$

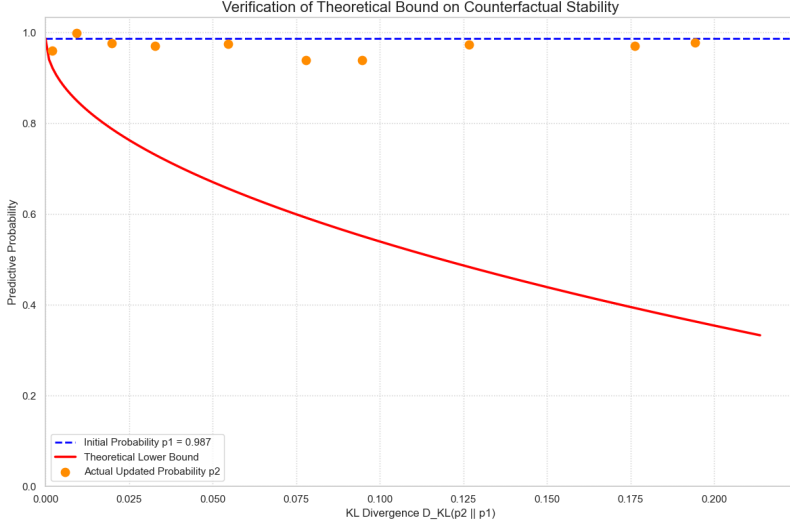


Figure 3: Verification of a closed form solution to the D_{KL} term presented in the inequality of Theorem 1 associated with the worked example in equation 2.

is necessary for a counterfactual under a model change to confidently remain a counterfactual. In Figure 3 we verify equation 2 showing the D_{KL} that is required for the theoretical bound to remain over 50% probability of the desired class, where:

$$D_{KL}(p_2(\omega|\cdot) \parallel p_1(\omega|\cdot)) \lesssim 0.111, \quad (2)$$

as we substitute δ for $1 - p(y'|\mathbf{x}', \mathcal{D}_{prev})$.

It is worth noting, this is not limited to the applications of counterfactuals as any δ or $p(y'|\mathbf{x}', \mathcal{D}_{prev})$ can be substituted. As clear from the proof of Theorem 1, under an observed predictive posterior $p_1(y'|\mathbf{x}', \mathcal{D}_{prev})$, we have the less conservative bound:

$$p_2(y'|\mathbf{x}', \mathcal{D}_{prev} \cup \mathcal{D}_{new}) \geq p_1(y'|\mathbf{x}', \mathcal{D}_{prev}) - 2 \cdot \sqrt{\frac{1}{2} D_{KL}(p_2(\omega|\cdot) \parallel p_1(\omega|\cdot))}.$$

We empirically explore this in the results section and the *supplementary material*. We can also ensure a conservative upper-bound on the predictive variance, leading to Theorem 2.

Theorem 2. *Let $Var_{\omega \sim p_1(\omega|\mathcal{D}_{prev})}[p_1(y'|\mathbf{x}', \omega)]$ be the variance in likelihood over a parametric posterior distribution $p_1(\omega|\mathcal{D}_{prev})$ given previously observed data \mathcal{D}_{prev} , where counterfactual \mathbf{x}' is ϵ -robust, such that:*

$$Var_{\omega \sim p_1(\omega|\mathcal{D}_{prev})}[p_1(y'|\mathbf{x}', \omega)] \leq \epsilon,$$

then under new observed data \mathcal{D}_{new} , providing a new posterior distribution of model parameters $p_2(\omega|\mathcal{D}_{prev} \cup \mathcal{D}_{new})$, we have:

$$Var_{\omega \sim p_2(\omega|\mathcal{D}_{prev} \cup \mathcal{D}_{new})}[p_2(y'|\mathbf{x}', \omega)] \leq \epsilon + 6 \cdot \sqrt{\frac{1}{2} D_{KL}(p_2(\omega|\cdot) \parallel p_1(\omega|\cdot))}.$$

Similarly, Theorem 2 shows that the variance degrades in a controlled way, bounded by ϵ plus a term dependent on KL divergence. By the proof of Theorem 2, we see that for an observed $Var_{\omega \sim p_1(\omega|\mathcal{D}_{prev})}[p_1(y'|\mathbf{x}', \omega)]$, we have:

$$Var_{\omega \sim p_2(\omega|\mathcal{D}_{prev} \cup \mathcal{D}_{new})}[p_2(y'|\mathbf{x}', \omega)] \leq Var_{\omega \sim p_1(\omega|\mathcal{D}_{prev})}[p_1(y'|\mathbf{x}', \omega)] + 6 \cdot \sqrt{\frac{1}{2} D_{KL}(p_2(\omega|\cdot) \parallel p_1(\omega|\cdot))}.$$

All missing proofs are provided in the *supplementary material*.

6 Experimental Setup

In the experimental setup, we explicitly consider Bayesian-based counterfactual explainers. Thus, we limit our scope on what we refer to as Schut (Schut et al., 2021) (using the “greedy” approach in algorithm 1 of their paper) and

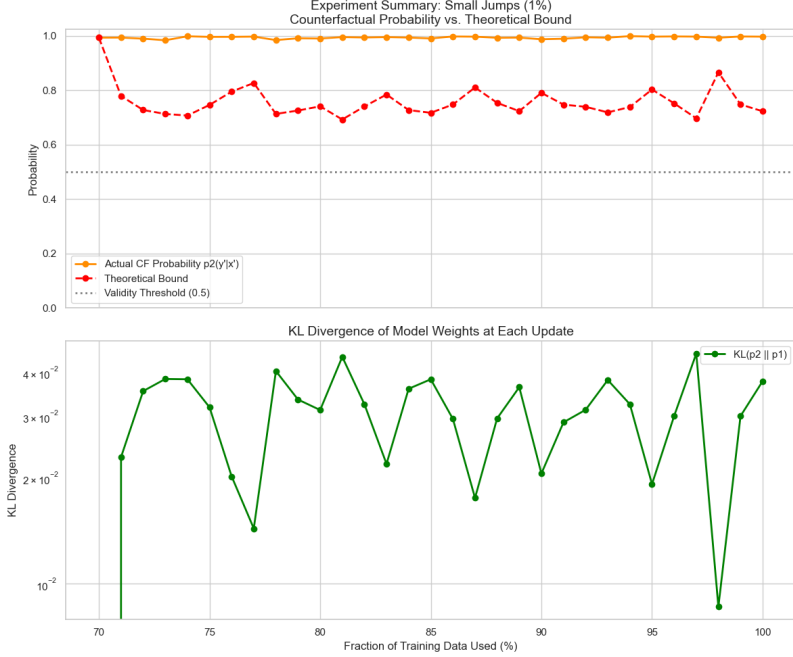


Figure 4: 1% increments in training data evaluating the theoretical bound vs computed approximate bound subject to the posterior over model weights.

BayesCF (Batten et al., 2025) due to their Bayesian nature. For each counterfactual method we adopt BNNs¹ and MC Dropout (see *supplementary material*) for all methods. Furthermore, for a fair comparison we accept all counterfactuals generated by the methods including our own, and do not explicitly accept δ -safe or ϵ -robust counterfactuals only.

We present evaluation metrics, model architecture and hyperparameter details in the *supplementary material*

6.1 Configuration

All experiments are conducted with a 3.50 GHz AMD Ryzen 5 5600 6-Core CPU and an NVIDIA GeForce RTX 4060 GPU. The implementation of each method was experimented using PyTorch.

6.2 Datasets

The datasets used in this paper follow standard counterfactual explanation literature (Batten et al., 2025; Schut et al., 2021; Noorani et al., 2025), where we adopt the MNIST, German Credit, Wisconsin Breast Cancer and Spambase datasets, we also include a MedMNIST (Yang et al., 2021, 2023) dataset, namely the PneumoniaMNIST. Dataset preprocessing details and further experiments are provided in the *supplementary material* with an example counterfactual explanation.

7 Results

7.1 Robustness Under Model Changes

To test the validity of Theorem 1, specifically the bound $p_1(y'|\mathbf{x}', \mathcal{D}_{prev}) - 2 \cdot \sqrt{\frac{1}{2} D_{KL}(p_2(\omega|\cdot) \| p_1(\omega|\cdot))}$, we carried out controlled experiments with minimal parameter change. We first train a neural network on 95% of the data to establish the initial posterior, $p_1(\omega|\cdot)$. Then, we incrementally update the model with an additional 1% of the training data. For this fine-tuning, only the final layer is updated, using a small learning rate (1e-5) to produce the new posterior, $p_2(\omega|\cdot)$. The KL divergence, $D_{KL}(p_2(\omega|\cdot) \| p_1(\omega|\cdot))$, is estimated by approximating both posteriors using a BNN for demonstration. We illustrate the relationship between the KL divergence, the theoretical bound, the counterfactual

¹we use the BNN implementation from torchbnn: <https://pypi.org/project/torchbnn/> (Lee et al., 2022)

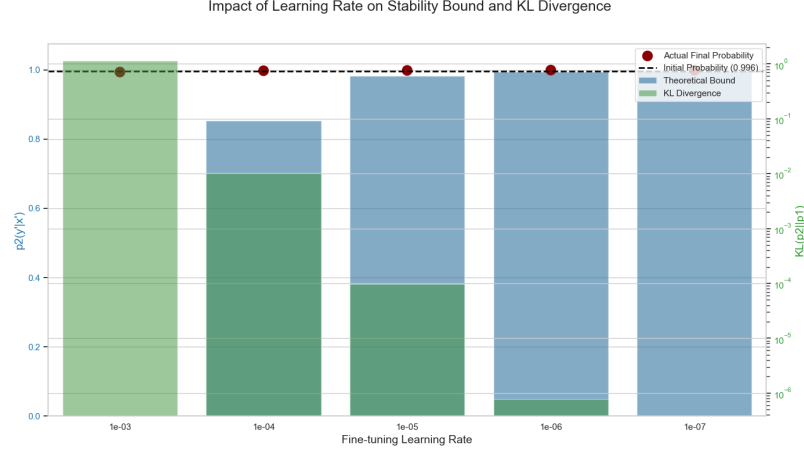


Figure 5: Comparison of the theoretical bound and the computed approximate bound under the posterior over model weights.

threshold, and the actual counterfactual probability under newly observed data in Figure 4 and Table 1. Additional experiments are presented in the *supplementary material*, where we vary the learning rate and data increment size, and analyze their effect on the KL divergence and the theoretical bound.

In Figure 5, we observe that a learning rate of 10^{-5} yields a reasonably tight bound. This confirms that sufficiently small learning rates are required in practice to obtain meaningful bounds. The bound becomes tighter as model changes decrease in size. This observation motivated our choice of learning rate for model changes in this work.

In summary, a small learning rate is necessary during data updates to ensure that parameter changes remain small enough for the bound to be meaningful.

Table 2: Performance metrics measured across all datasets. The best performing method is highlighted in **bold** text. The experiments are run over 5 runs and the *mean* and *standard deviation* are recorded. Each run is evaluated over 100 instances from the test data. These results use **BNN**.

Dataset	Metric	PSCE (Ours)	BayesCF	Schut
Credit	IM1 (↓)	0.6561 ± 0.0603	0.8311 ± 0.0289	0.9042 ± 0.0222
	Implausibility (↓)	8.4606 ± 0.2683	10.1530 ± 0.3799	10.8363 ± 0.1218
	Robustness Ratio 1e-3 (↓)	0.1400 ± 0.0203	0.1461 ± 0.0168	0.2318 ± 0.0304
	Validity % (↑)	100.0 ± 0.0	100.0 ± 0.0	100.0 ± 0.0
Breast Cancer	IM1 (↓)	1.5540 ± 0.2427	1.1957 ± 0.0507	1.1151 ± 0.0362
	Implausibility (↓)	5.7579 ± 0.0439	7.2014 ± 0.0423	7.4072 ± 0.0333
	Robustness Ratio 1e-3 (↓)	0.1566 ± 0.0152	0.3867 ± 0.0306	0.3050 ± 0.0211
	Validity % (↑)	86.8±3.2	78.4±3.5	84.8±1.9
MNIST	IM1 (↓)	0.9768 ± 0.1598	1.6408 ± 0.1267	1.2298 ± 0.0526
	Implausibility (↓)	28.1567 ± 0.2665	35.7763 ± 0.0737	31.2247 ± 0.2067
	Robustness Ratio 1e-3 (↓)	0.7822 ± 0.0289	1.0191 ± 0.0463	0.9011 ± 0.0170
	Validity % (↑)	98.2±1.6	67.6±5.4	96.0±1.8
Spam	IM1 (↓)	0.7387 ± 0.0578	1.0948 ± 0.0218	0.9137 ± 0.0299
	Implausibility (↓)	6.1781 ± 0.0312	9.4032 ± 0.0471	12.9145 ± 0.1061
	Robustness Ratio 1e-3 (↓)	0.1028 ± 0.0099	0.1507 ± 0.0124	0.2046 ± 0.0083
	Validity % (↑)	96.0 ± 3.3	100.0 ± 0.0	98.6±0.5
PneumoniaMNIST	IM1 (↓)	0.630 ± 0.095	1.062 ± 0.009	1.157 ± 0.024
	Implausibility (↓)	4.465 ± 0.332	5.687 ± 0.027	5.350 ± 0.019
	Robustness Ratio 1e-3 (↓)	0.255 ± 0.020	1.191 ± 0.009	1.015 ± 0.033
	Validity % (↑)	99.8±0.4	98.4±1.5	91.2±3.6

Table 3: Performance metrics measured across all datasets. The best performing method is highlighted in **bold** text. The experiments are run over 5 runs and the *mean* and *standard deviation* are recorded. Each run is evaluated over 100 instances from the test data. These results use **MC Dropout**.

Dataset	Metric	PSCE (Ours)	BayesCF	Schut
Credit	IM1 (↓)	0.7383 ± 0.0341	1.0767 ± 0.0214	0.9251 ± 0.0320
	Implausibility (↓)	8.6113 ± 0.1494	9.3615 ± 0.0543	9.9943 ± 0.2124
	Robustness Ratio 1e-3 (↓)	0.0622 ± 0.0103	0.1219 ± 0.0106	0.1418 ± 0.0208
	Validity % (↑)	100.0±0.0	66.8± 5.2	100.0±0.0
Breast Cancer	IM1 (↓)	0.6932 ± 0.0911	1.1300 ± 0.0306	1.0332 ± 0.0340
	Implausibility (↓)	5.6275 ± 0.0627	7.1505 ± 0.0323	7.2913 ± 0.0354
	Robustness Ratio 1e-3 (↓)	0.0800 ± 0.0047	0.0539 ± 0.0104	0.1045 ± 0.0105
	Validity % (↑)	97.2±1.6	79.2±5.0	90.4±0.8
MNIST	IM1 (↓)	0.9273 ± 0.0172	1.6426 ± 0.2774	1.2373 ± 0.0392
	Implausibility (↓)	27.0337 ± 0.4335	32.9022 ± 0.2163	31.3665 ± 0.1397
	Robustness Ratio 1e-3 (↓)	0.6493 ± 0.0496	0.9918 ± 0.0471	1.0696 ± 0.0412
	Validity % (↑)	99.6±0.8	47.8±3.3	100.0 ± 0.0
Spam	IM1 (↓)	0.8967 ± 0.0316	1.4798 ± 0.0122	1.2756 ± 0.0225
	Implausibility (↓)	7.2057 ± 0.0618	9.4627 ± 0.0442	10.0120 ± 0.0461
	Robustness Ratio 1e-3 (↓)	0.0429 ± 0.0063	0.0868 ± 0.0092	0.0870 ± 0.0151
	Validity % (↑)	91.8 ± 4.5	79.0±4.0	99.0±0.0
PneumoniaMNIST	IM1 (↓)	0.545 ± 0.102	1.062 ± 0.012	1.031 ± 0.007
	Implausibility (↓)	4.489 ± 0.149	5.647 ± 0.037	6.066 ± 0.138
	Robustness Ratio 1e-3 (↓)	0.098 ± 0.017	0.597 ± 0.030	0.770 ± 0.034
	Validity % (↑)	99.4±0.5	100.0±0.0	100.0±0.0

7.2 Comparison Under Key Metrics

In Table 17 and Table 18, we observe the performance of the proposed PSCE when compared against existing Bayesian CEs. Here we can see our approach mostly exhibits superior performance across key metrics.

8 Conclusion

This paper introduces the PSCE method for Bayesian inspired CEs. We show both theoretically and empirically, the robustness of CEs under our method with respect to model changes. Our approach empirically performs better than existing Bayesian inspired counterfactual explanation methods on a collection of core datasets that are used within counterfactual literature.

References

Altmeyer, P., Farmanbar, M., van Deursen, A., and Liem, C. C. S. (2024). Faithful model explanations through energy-constrained conformal counterfactuals. In *Proceedings of the Thirty-Eighth AAAI Conference on Artificial Intelligence and Thirty-Sixth Conference on Innovative Applications of Artificial Intelligence and Fourteenth Symposium on Educational Advances in Artificial Intelligence, AAAI'24/IAAI'24/EAAI'24*. AAAI Press.

Batten, B., Leofante, F., Paoletti, N., Lomuscio, A., and Hosseini, M. (2025). Uncertainty-aware counterfactual explanations using bayesian neural nets.

Deng, L. (2012). The mnist database of handwritten digit images for machine learning research [best of the web]. *IEEE Signal Processing Magazine*, 29(6):141–142.

Gal, Y. and Ghahramani, Z. (2016). Dropout as a bayesian approximation: Representing model uncertainty in deep learning. In Balcan, M. F. and Weinberger, K. Q., editors, *Proceedings of The 33rd International Conference on Machine Learning*, volume 48 of *Proceedings of Machine Learning Research*, pages 1050–1059, New York, New York, USA. PMLR.

Hamman, F., Noorani, E., Mishra, S., Magazzeni, D., and Dutta, S. (2023). Robust counterfactual explanations for neural networks with probabilistic guarantees. In Krause, A., Brunskill, E., Cho, K., Engelhardt, B., Sabato, S., and

Scarlett, J., editors, *International Conference on Machine Learning, ICML 2023, 23-29 July 2023, Honolulu, Hawaii, USA*, volume 202 of *Proceedings of Machine Learning Research*, pages 12351–12367. PMLR.

Hoi, S. C. H., Sahoo, D., Lu, J., and Zhao, P. (2018). Online learning: A comprehensive survey.

Jiang, J., Leofante, F., Rago, A., and Toni, F. (2024). Robust counterfactual explanations in machine learning: a survey. In *Proceedings of the Thirty-Third International Joint Conference on Artificial Intelligence, IJCAI '24*.

Kingma, D. P. and Ba, J. (2014). Adam: A method for stochastic optimization. *CoRR*, abs/1412.6980.

Kingma, D. P. and Welling, M. (2014). Auto-encoding variational bayes. In Bengio, Y. and LeCun, Y., editors, *2nd International Conference on Learning Representations, ICLR 2014, Banff, AB, Canada, April 14-16, 2014, Conference Track Proceedings*.

LeCun, Y., Bottou, L., Bengio, Y., and Haffner, P. (1998). Gradient-based learning applied to document recognition. *Proc. IEEE*, 86:2278–2324.

Lee, S., Kim, H., and Lee, J. (2022). Graddiv: Adversarial robustness of randomized neural networks via gradient diversity regularization. *IEEE Transactions on Pattern Analysis and Machine Intelligence*.

Mothilal, R. K., Sharma, A., and Tan, C. (2020). Explaining machine learning classifiers through diverse counterfactual explanations. In *Proceedings of the 2020 Conference on Fairness, Accountability, and Transparency, FAT* '20*, page 607–617, New York, NY, USA. Association for Computing Machinery.

Noorani, E., Dissanayake, P., Hamman, F., and Dutta, S. (2025). Counterfactual explanations for model ensembles using entropic risk measures. In *Proceedings of the 24th International Conference on Autonomous Agents and Multiagent Systems, AAMAS '25*, page 1566–1575, Richland, SC. International Foundation for Autonomous Agents and Multiagent Systems.

Schut, L., Key, O., McGrath, R., Costabello, L., Sacaleanu, B., Corcoran, M., and Gal, Y. (2021). Generating interpretable counterfactual explanations by implicit minimisation of epistemic and aleatoric uncertainties. In *International Conference on Artificial Intelligence and Statistics*.

Sokol, K. and Hüllermeier, E. (2025). All you need for counterfactual explainability is principled and reliable estimate of aleatoric and epistemic uncertainty.

Stepka, I., Stefanowski, J., and Lango, M. (2025). Counterfactual explanations with probabilistic guarantees on their robustness to model change. In *Proceedings of the 31st ACM SIGKDD Conference on Knowledge Discovery and Data Mining V.1, KDD '25*, page 1277–1288, New York, NY, USA. Association for Computing Machinery.

Tran, D., Dusenberry, M. W., van der Wilk, M., and Hafner, D. (2019). *Bayesian layers: a module for neural network uncertainty*. Curran Associates Inc., Red Hook, NY, USA.

Upadhyay, S., Joshi, S., and Lakkaraju, H. (2021). Towards robust and reliable algorithmic recourse. In Beygelzimer, A., Dauphin, Y., Liang, P., and Vaughan, J. W., editors, *Advances in Neural Information Processing Systems*.

van de Ven, G. M., Tuytelaars, T., and Tolias, A. S. (2022). Three types of incremental learning. *Nature Machine Intelligence*, 4(12):1185–1197.

Van Looveren, A. and Klaise, J. (2021). Interpretable counterfactual explanations guided by prototypes. In *Machine Learning and Knowledge Discovery in Databases. Research Track: European Conference, ECML PKDD 2021, Bilbao, Spain, September 13–17, 2021, Proceedings, Part II*, page 650–665, Berlin, Heidelberg. Springer-Verlag.

Wachter, S., Mittelstadt, B., and Russell, C. (2018). Counterfactual explanations without opening the black box: Automated decisions and the gdpr. *Harvard journal of law & technology*, 31:841–887.

Yang, J., Shi, R., and Ni, B. (2021). Medmnist classification decathlon: A lightweight automl benchmark for medical image analysis. In *IEEE 18th International Symposium on Biomedical Imaging (ISBI)*, pages 191–195.

Yang, J., Shi, R., Wei, D., Liu, Z., Zhao, L., Ke, B., Pfister, H., and Ni, B. (2023). Medmnist v2-a large-scale lightweight benchmark for 2d and 3d biomedical image classification. *Scientific Data*, 10(1):41.

A MISSING PROOFS

A.1 Proof of Theorem 1

Recalling the Theorem for readability: Let $p_1(\omega|\mathcal{D}_{\text{prev}})$ be a probabilistic model's posterior distribution over its parameters ω . After a data update, the new posterior is $p_2(\omega|\mathcal{D}_{\text{prev}} \cup \mathcal{D}_{\text{new}})$. Given the initial posterior predictive probability for a class y' given a counterfactual \mathbf{x}' is at least $p_1(y'|\mathbf{x}', \mathcal{D}_{\text{prev}}) \geq 1 - \delta$, then the updated posterior predictive probability is bounded such that:

$$p_2(y'|\mathbf{x}', \mathcal{D}_{\text{prev}} \cup \mathcal{D}_{\text{new}}) \geq (1 - \delta) - 2 \cdot \sqrt{\frac{1}{2} D_{\text{KL}}(p_2(\omega|\cdot) \| p_1(\omega|\cdot))},$$

where, $p_2(\omega|\cdot) = p_2(\omega|\mathcal{D}_{\text{prev}} \cup \mathcal{D}_{\text{new}})$ and $p_1(\omega|\cdot) = p_1(\omega|\mathcal{D}_{\text{prev}})$.

Proof. Let $\pi_2 = p_2(y'|\mathbf{x}', \mathcal{D}_{\text{prev}} \cup \mathcal{D}_{\text{new}})$ and $\pi_1 = p_1(y'|\mathbf{x}', \mathcal{D}_{\text{prev}})$. We also let $f(\omega) = p(y'|\mathbf{x}', \omega)$. Then,

$$\begin{aligned} |\pi_2 - \pi_1| &= |\mathbb{E}_{\omega \sim p_2(\omega|\cdot)}[f(\omega)] - \mathbb{E}_{\omega \sim p_1(\omega|\cdot)}[f(\omega)]| \\ &= \left| \int f(\omega)p_2(\omega|\cdot)d\omega - \int f(\omega)p_1(\omega|\cdot)d\omega \right| \\ &= \left| \int f(\omega)(p_2(\omega|\cdot) - p_1(\omega|\cdot))d\omega \right|. \end{aligned}$$

By properties of the integral we can note that:

$$\left| \int f(\omega)(p_2(\omega|\cdot) - p_1(\omega|\cdot))d\omega \right| \leq \sup_{\omega} |f(\omega)| \cdot \int |p_2(\omega|\cdot) - p_1(\omega|\cdot)|d\omega$$

then by the total variation (TV), namely: $\text{TV}(p_2(\omega|\cdot), p_1(\omega|\cdot)) = \frac{1}{2} \int |p_2(\omega|\cdot) - p_1(\omega|\cdot)|$, we have:

$$|\pi_2 - \pi_1| \leq 2 \cdot \sup_{\omega} |f(\omega)| \cdot \text{TV}(p_2(\omega|\cdot), p_1(\omega|\cdot)),$$

Then by Pinsker's inequality, we have:

$$\text{TV}(p_2(\omega|\cdot), p_1(\omega|\cdot)) \leq \sqrt{\frac{1}{2} D_{\text{KL}}(p_2(\omega|\cdot) \| p_1(\omega|\cdot))},$$

thus,

$$|\pi_2 - \pi_1| \leq 2 \cdot \sup_{\omega} |f(\omega)| \cdot \sqrt{\frac{1}{2} D_{\text{KL}}(p_2(\omega|\cdot) \| p_1(\omega|\cdot))}.$$

Since $\pi_1 \in [1 - \delta, 1]$ (implying that $\pi_1 \geq 1 - \delta$) for some $\delta \in [0, 1]$, that is all that is necessary to establish the lower bound:

$$\begin{aligned} \pi_2 &\geq \pi_1 - 2 \cdot \sup_{\omega} |f(\omega)| \cdot \sqrt{\frac{1}{2} D_{\text{KL}}(p_2(\omega|\cdot) \| p_1(\omega|\cdot))} \\ &\geq (1 - \delta) - 2 \cdot \sup_{\omega} |f(\omega)| \cdot \sqrt{\frac{1}{2} D_{\text{KL}}(p_2(\omega|\cdot) \| p_1(\omega|\cdot))}, \end{aligned}$$

finally, since we know that $p(y'|\mathbf{x}', \omega) \in [0, 1]$, then:

$$(1 - \delta) - 2 \cdot \sqrt{\frac{1}{2} D_{\text{KL}}(p_2(\omega|\cdot) \| p_1(\omega|\cdot))},$$

providing the final bound. \square

A.2 Proof of Theorem 2

We begin by again recalling Theorem 2 for readability: Let $\text{Var}_{\omega \sim p_1(\omega | \mathcal{D}_{\text{prev}})}[p_1(y' | \mathbf{x}', \omega)]$ be the variance in likelihood over a parametric distribution $p_1(\omega | \mathcal{D}_{\text{prev}})$ given previously observed data $\mathcal{D}_{\text{prev}}$, where counterfactual \mathbf{x}' is ϵ -robust, such that:

$$\text{Var}_{\omega \sim p_1(\omega | \mathcal{D}_{\text{prev}})}[p_1(y' | \mathbf{x}', \omega)] \leq \epsilon,$$

then under new observed data \mathcal{D}_{new} , providing a new posterior distribution of model parameters $p_2(\omega | \mathcal{D}_{\text{prev}} \cup \mathcal{D}_{\text{new}})$, we have:

$$\text{Var}_{\omega \sim p_2(\omega | \mathcal{D}_{\text{prev}} \cup \mathcal{D}_{\text{new}})}[p_2(y' | \mathbf{x}', \omega)] \leq \epsilon + 6 \cdot \sqrt{\frac{1}{2} D_{\text{KL}}(p_2(\omega | \cdot) \| p_1(\omega | \cdot))}.$$

Proof. By adopting the previous notation from the proof of Theorem 1 for simplicity, such that $f(\omega) := p(y' | \mathbf{x}', \omega)$. We can observe that:

$$\begin{aligned} \text{Var}_{\omega \sim p_1(\omega | \mathcal{D}_{\text{prev}})}[f(\omega)] &= \mathbb{E}[(f(\omega) - \mathbb{E}[f(\omega)])^2] \\ &= \mathbb{E}[f(\omega)^2 - 2f(\omega)\mathbb{E}[f(\omega)] + \mathbb{E}[f(\omega)]^2] \\ &= \mathbb{E}[f(\omega)^2] - 2\mathbb{E}[f(\omega)]\mathbb{E}[f(\omega)] + \mathbb{E}[f(\omega)]^2 \\ &= \mathbb{E}[f(\omega)^2] - 2\mathbb{E}[f(\omega)]^2 + \mathbb{E}[f(\omega)]^2 \\ &= \mathbb{E}[f(\omega)^2] - \mathbb{E}[f(\omega)]^2 : \mathbb{E} := \mathbb{E}_{\omega \sim p_1(\omega | \mathcal{D}_{\text{prev}})} \end{aligned}$$

Similarly,

$$\text{Var}_{\omega \sim p_2(\omega | \mathcal{D}_{\text{prev}} \cup \mathcal{D}_{\text{new}})}[f(\omega)] = \mathbb{E}[f(\omega)^2] - \mathbb{E}[f(\omega)]^2 : \mathbb{E} := \mathbb{E}_{\omega \sim p_2(\omega | \mathcal{D}_{\text{prev}} \cup \mathcal{D}_{\text{new}})}$$

Then, similar to Theorem 1, we aim to find a bound on $|\text{Var}_{\omega \sim p_2(\omega | \cdot)}[f(\omega)] - \text{Var}_{\omega \sim p_1(\omega | \cdot)}[f(\omega)]|$, where $p_2(\omega | \cdot) = p_2(\omega | \mathcal{D}_{\text{prev}} \cup \mathcal{D}_{\text{new}})$ and $p_1(\omega | \cdot) = p_1(\omega | \mathcal{D}_{\text{prev}})$, such that:

$$\begin{aligned} &|\text{Var}_{\omega \sim p_2(\omega | \cdot)}[f(\omega)] - \text{Var}_{\omega \sim p_1(\omega | \cdot)}[f(\omega)]| = \\ &|(\mathbb{E}_{\omega \sim p_2(\omega | \cdot)}[f(\omega)^2] - \mathbb{E}_{\omega \sim p_2(\omega | \cdot)}[f(\omega)]^2) - (\mathbb{E}_{\omega \sim p_1(\omega | \cdot)}[f(\omega)^2] - \mathbb{E}_{\omega \sim p_1(\omega | \cdot)}[f(\omega)]^2)| \\ &\leq |\mathbb{E}_{\omega \sim p_2(\omega | \cdot)}[f(\omega)^2] - \mathbb{E}_{\omega \sim p_1(\omega | \cdot)}[f(\omega)^2]| + |\mathbb{E}_{\omega \sim p_2(\omega | \cdot)}[f(\omega)]^2 - \mathbb{E}_{\omega \sim p_1(\omega | \cdot)}[f(\omega)]^2| \end{aligned}$$

by the triangle inequality. Then observing $f(\omega) \in [0, 1]$, this implies that $f(\omega)^2 \in [0, 1]$, therefore, by total variation (TV) as per Theorem 1, we similarly observe that:

$$|\mathbb{E}_{\omega \sim p_2(\omega | \cdot)}[f(\omega)^2] - \mathbb{E}_{\omega \sim p_1(\omega | \cdot)}[f(\omega)^2]| \leq 2 \cdot \sqrt{\frac{1}{2} D_{\text{KL}}(p_2 \| p_1(\omega | \cdot))},$$

we can then proceed to consider the term

$$|\mathbb{E}_{\omega \sim p_2(\omega | \cdot)}[f(\omega)]^2 - \mathbb{E}_{\omega \sim p_1(\omega | \cdot)}[f(\omega)]^2| = |\mathbb{E}_{\omega \sim p_2(\omega | \cdot)}[f(\omega)] - \mathbb{E}_{\omega \sim p_1(\omega | \cdot)}[f(\omega)]| |\mathbb{E}_{\omega \sim p_2(\omega | \cdot)}[f(\omega)] + \mathbb{E}_{\omega \sim p_1(\omega | \cdot)}[f(\omega)]|$$

then since, we know that both, $0 \leq \mathbb{E}_{\omega \sim p_2(\omega | \cdot)}[f(\omega)] \leq 1$ and $0 \leq \mathbb{E}_{\omega \sim p_1(\omega | \cdot)}[f(\omega)] \leq 1$, we can see that:

$$\begin{aligned} &|\mathbb{E}_{\omega \sim p_2(\omega | \cdot)}[f(\omega)] - \mathbb{E}_{\omega \sim p_1(\omega | \cdot)}[f(\omega)]| \underbrace{|\mathbb{E}_{\omega \sim p_2(\omega | \cdot)}[f(\omega)] + \mathbb{E}_{\omega \sim p_1(\omega | \cdot)}[f(\omega)]|}_{\leq 2} \implies |\mathbb{E}_{\omega \sim p_2(\omega | \cdot)}[f(\omega)]^2 - \mathbb{E}_{\omega \sim p_1(\omega | \cdot)}[f(\omega)]^2| \\ &\leq 2 \cdot |\mathbb{E}_{\omega \sim p_2(\omega | \cdot)}[f(\omega)] - \mathbb{E}_{\omega \sim p_1(\omega | \cdot)}[f(\omega)]| \leq 4 \cdot \sqrt{\frac{1}{2} D_{\text{KL}}(p_2(\omega | \cdot) \| p_1(\omega | \cdot))} \\ &\implies |\mathbb{E}_{\omega \sim p_2(\omega | \cdot)}[f(\omega)]^2 - \mathbb{E}_{\omega \sim p_1(\omega | \cdot)}[f(\omega)]^2| \leq 4 \cdot \sqrt{\frac{1}{2} D_{\text{KL}}(p_2(\omega | \cdot) \| p_1(\omega | \cdot))} \end{aligned}$$

then by summing over the constants for the individual bounds, we have the final bound:

$$|\text{Var}_{\omega \sim p_2(\omega | \cdot)}[f(\omega)] - \text{Var}_{\omega \sim p_1(\omega | \cdot)}[f(\omega)]| \leq 6 \cdot \sqrt{\frac{1}{2} D_{\text{KL}}(p_2 \| p_1(\omega | \cdot))}$$

and therefore:

$$\begin{aligned} \text{Var}_{\omega \sim p_2(\omega | \cdot)}[f(\omega)] &\leq \text{Var}_{\omega \sim p_1(\omega | \cdot)}[f(\omega)] + 6 \cdot \sqrt{\frac{1}{2} D_{\text{KL}}(p_2(\omega | \cdot) \| p_1(\omega | \cdot))} \\ &\implies \text{Var}_{\omega \sim p_2(\omega | \cdot)}[f(\omega)] \leq \epsilon + 6 \cdot \sqrt{\frac{1}{2} D_{\text{KL}}(p_2 \| p_1(\omega | \cdot))} \end{aligned}$$

□

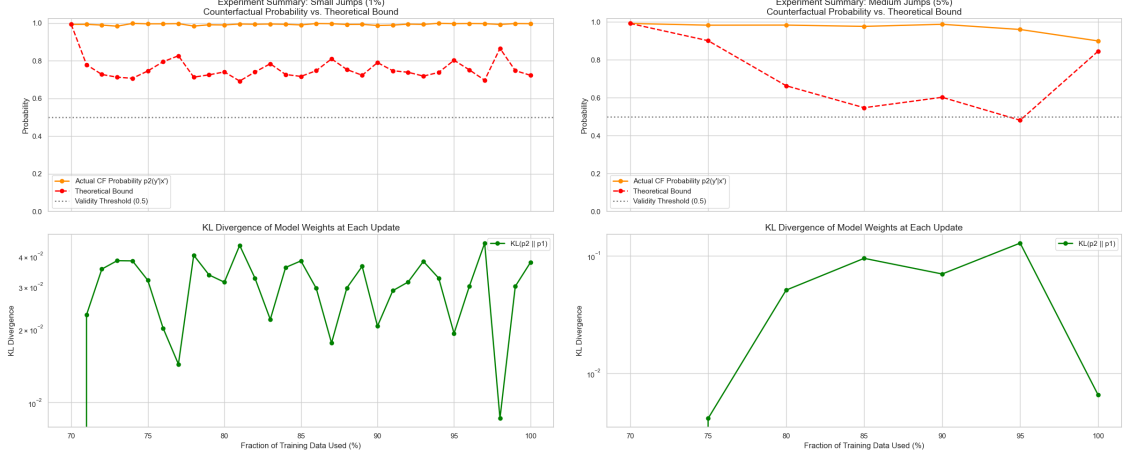


Figure 6: 1% and 5% increments in training data.

B ELBO Derivation

We provide the standard ELBO derivation for completeness. Recall, we have that:

$$\begin{aligned}
\log p(\mathbf{x}) &= \log \int p_{\theta}(\mathbf{x}|\mathbf{z})p(\mathbf{z}) \\
&= \log \int q_{\phi}(\mathbf{z}|\mathbf{x}) \frac{p_{\theta}(\mathbf{x}|\mathbf{z})p(\mathbf{z})}{q_{\phi}(\mathbf{z}|\mathbf{x})} d\mathbf{z} \\
&\geq \int q_{\phi}(\mathbf{z}|\mathbf{x}) \log \left(\frac{p_{\theta}(\mathbf{x}|\mathbf{z})p(\mathbf{z})}{q_{\phi}(\mathbf{z}|\mathbf{x})} \right) d\mathbf{z} \\
&= \mathbb{E}_{q_{\phi}(\mathbf{z}|\mathbf{x})} \left[\log \left(\frac{p_{\theta}(\mathbf{x}|\mathbf{z})p(\mathbf{z})}{q_{\phi}(\mathbf{z}|\mathbf{x})} \right) \right] \\
&= \mathbb{E}_{q_{\phi}(\mathbf{z}|\mathbf{x})} [\log p_{\theta}(\mathbf{x}|\mathbf{z})] + \mathbb{E}_{q_{\phi}(\mathbf{z}|\mathbf{x})} [\log p(\mathbf{z})] - \mathbb{E}_{q_{\phi}(\mathbf{z}|\mathbf{x})} [\log q_{\phi}(\mathbf{z}|\mathbf{x})] \\
&= \mathbb{E}_{q_{\phi}(\mathbf{z}|\mathbf{x})} [\log p_{\theta}(\mathbf{x}|\mathbf{z})] + \left(\int q_{\phi}(\mathbf{z}|\mathbf{x}) \log \left(\frac{p(\mathbf{z})}{q_{\phi}(\mathbf{z}|\mathbf{x})} \right) d\mathbf{z} \right) \\
&= \mathbb{E}_{q_{\phi}(\mathbf{z}|\mathbf{x})} [\log p_{\theta}(\mathbf{x}|\mathbf{z})] + \left(-D_{\text{KL}}(q_{\phi}(\mathbf{z}|\mathbf{x})\|p(\mathbf{z})) \right) \\
&= \mathbb{E}_{q_{\phi}(\mathbf{z}|\mathbf{x})} [\log p_{\theta}(\mathbf{x}|\mathbf{z})] - D_{\text{KL}}(q_{\phi}(\mathbf{z}|\mathbf{x})\|p(\mathbf{z})) \\
&= \text{ELBO} \\
\implies \log p(\mathbf{x}) &\geq \text{ELBO} = \mathbb{E}_{q_{\phi}(\mathbf{z}|\mathbf{x})} [\log p_{\theta}(\mathbf{x}|\mathbf{z})] - D_{\text{KL}}(q_{\phi}(\mathbf{z}|\mathbf{x})\|p(\mathbf{z})).
\end{aligned}$$

Completing the derivation. In the main paper, we use line 5 as our representation of the loss function and indeed follows the standard definition of ELBO.

C Robustness of Bounds in Practice

In the main manuscript, we provide a simple analysis of the robustness under a small model change to the final layer of a network under new data. In Figures 6, we illustrate the theoretical bound against the actual prediction probability under different learning different size data increments.

To extrapolate on the main manuscript, we work through the algebra on the RHS of the bound in Theorem 1. In practice, we wish to have a rational bounds above ≥ 0.5 for a valid counterfactual, thus we can solve for this explicitly:

$$(1 - \delta) - 2 \cdot \sqrt{\frac{1}{2} D_{\text{KL}}(p_2(\omega|\cdot)\|p_1(\omega|\cdot))} \geq 0.5$$

Then, working through the algebra to isolate the D_{KL} term, we have:

$$\begin{aligned}
 (1 - \delta) - 2 \cdot \sqrt{\frac{1}{2} D_{\text{KL}}(p_2(\omega|\cdot) || p_1(\omega|\cdot))} &\geq 0.5 \\
 \implies (1 - \delta) - 2 \cdot \sqrt{\frac{1}{2} D_{\text{KL}}(p_2(\omega|\cdot) || p_1(\omega|\cdot))} - (1 - \delta) &\geq 0.5 - (1 - \delta) \\
 \implies -2 \cdot \sqrt{\frac{1}{2} D_{\text{KL}}(p_2(\omega|\cdot) || p_1(\omega|\cdot))} &\geq \delta - 0.5
 \end{aligned}$$

multiplying both sides by -1, we have:

$$\begin{aligned}
 (-1) \left(-2 \cdot \sqrt{\frac{1}{2} D_{\text{KL}}(p_2(\omega|\cdot) || p_1(\omega|\cdot))} \right) &\leq (-1)(\delta - 0.5) \\
 \implies 2 \cdot \sqrt{\frac{1}{2} D_{\text{KL}}(p_2(\omega|\cdot) || p_1(\omega|\cdot))} &\leq 0.5 - \delta \\
 \implies \frac{2 \cdot \sqrt{\frac{1}{2} D_{\text{KL}}(p_2(\omega|\cdot) || p_1(\omega|\cdot))}}{2} &\leq \frac{(0.5 - \delta)}{2} \\
 \implies \sqrt{\frac{1}{2} D_{\text{KL}}(p_2(\omega|\cdot) || p_1(\omega|\cdot))} &\leq \frac{(0.5 - \delta)}{2} \\
 \implies \left(\sqrt{\frac{1}{2} D_{\text{KL}}(p_2(\omega|\cdot) || p_1(\omega|\cdot))} \right)^2 &\leq \left(\frac{(0.5 - \delta)}{2} \right)^2 \\
 \implies \frac{1}{2} D_{\text{KL}}(p_2(\omega|\cdot) || p_1(\omega|\cdot)) &\leq \left(\frac{(0.5 - \delta)}{2} \right)^2 \\
 \implies 2 \cdot \left(\frac{1}{2} D_{\text{KL}}(p_2(\omega|\cdot) || p_1(\omega|\cdot)) \right) &\leq 2 \cdot \left(\frac{(0.5 - \delta)}{2} \right)^2 \\
 \implies D_{\text{KL}}(p_2(\omega|\cdot) || p_1(\omega|\cdot)) &\leq 2 \cdot \left(\frac{(0.5 - \delta)}{2} \right)^2 \\
 \implies D_{\text{KL}}(p_2(\omega|\cdot) || p_1(\omega|\cdot)) &\leq \frac{(0.5 - \delta)^2}{2}
 \end{aligned}$$

Thus providing an ideal value for $D_{\text{KL}}(p_2(\omega|\cdot) || p_1(\omega|\cdot))$, if one wishes to ensure a counterfactual is equal to or over the probabilistic decision threshold for a counterfactual instance (0.5) upon a model change. Plugging in a value for $\delta = 0.05$, we can see for example, a counterfactual instance under model changes will remain a counterfactual instance, such that:

$$\begin{aligned}
 D_{\text{KL}}(p_2(\omega|\cdot) || p_1(\omega|\cdot)) &\leq \frac{(0.5 - 0.05)^2}{2} \\
 \implies D_{\text{KL}}(p_2(\omega|\cdot) || p_1(\omega|\cdot)) &\leq 0.10125
 \end{aligned}$$

Thus, in the context of the δ used in this work (0.05) (one could also use $p_1(y'|\mathbf{x}', \mathcal{D}_{\text{prev}})$ in place of δ), the KL divergence between parameters of a model change must be ≤ 0.10125 to have a meaningful bound in the context of counterfactuals. In practice, $p_2(\omega|\cdot)$ and $p_1(\omega|\cdot)$ are approximated.

D Robustness of Variance to Model Changes

We can go through a similar exercise to explore $\epsilon + 6 \cdot \sqrt{\frac{1}{2} D_{\text{KL}}(p_2(\omega|\cdot) || p_1(\omega|\cdot))}$, that is, consider we wish to have:

$$\epsilon + 6 \cdot \sqrt{\frac{1}{2} D_{\text{KL}}(p_2(\omega|\cdot) || p_1(\omega|\cdot))} \leq 0.01$$

Then, again by isolating the D_{KL} term, we go through the algebra such that:

$$\begin{aligned}
& \epsilon + 6\sqrt{\frac{1}{2}D_{\text{KL}}(p_2(\omega|\cdot)\|p_1(\omega|\cdot))} \leq 0.01 \\
\implies & 6\sqrt{\frac{1}{2}D_{\text{KL}}(p_2(\omega|\cdot)\|p_1(\omega|\cdot))} \leq 0.01 - \epsilon \\
\implies & -6\sqrt{\frac{1}{2}D_{\text{KL}}(p_2(\omega|\cdot)\|p_1(\omega|\cdot))} \geq \epsilon - 0.01 \\
\implies & \sqrt{\frac{1}{2}D_{\text{KL}}(p_2(\omega|\cdot)\|p_1(\omega|\cdot))} \leq \frac{\epsilon - 0.01}{-6} \\
\implies & \left(\sqrt{\frac{1}{2}D_{\text{KL}}(p_2(\omega|\cdot)\|p_1(\omega|\cdot))}\right)^2 \leq \left(\frac{\epsilon - 0.01}{-6}\right)^2 \\
\implies & \frac{1}{2}D_{\text{KL}}(p_2(\omega|\cdot)\|p_1(\omega|\cdot)) \leq \left(\frac{\epsilon - 0.01}{-6}\right)^2 \\
\implies & 2 \cdot \left(\frac{1}{2}D_{\text{KL}}(p_2(\omega|\cdot)\|p_1(\omega|\cdot))\right) \leq 2 \cdot \left(\frac{\epsilon - 0.01}{-6}\right)^2 \\
\implies & D_{\text{KL}}(p_2(\omega|\cdot)\|p_1(\omega|\cdot)) \leq \frac{2(\epsilon - 0.01)^2}{36} = \frac{(\epsilon - 0.01)^2}{18}
\end{aligned}$$

We do not proceed to provide more examples, but a similar exercise to Appendix C can be performed.

E Estimating KL Divergence Between BNN Posteriors

Our robustness bounds (Theorems 1 and 2) require computing the KL divergence between the posterior weight distributions before and after a model change. Since we use BNNs with mean-field Gaussian approximations (via `torchbnn`), each parameter is modeled independently as

$$p(\omega_i) = \mathcal{N}(\mu_i, \sigma_i^2),$$

where μ_i and σ_i^2 are learned by the BNN. We extract the means and variances from all `BayesLinear` layers using:

```
def get_bnn_posterior_params(model):
    mus, variances = [], []
    with torch.no_grad():
        for module in model.modules():
            if isinstance(module, bnn.BayesLinear):
                mus.append(module.weight_mu.flatten())
                variances.append(torch.exp(module.weight_log_sigma * 2).flatten())
            if module.bias_mu is not None:
                mus.append(module.bias_mu.flatten())
                variances.append(torch.exp(module.bias_log_sigma * 2).flatten())
    return torch.cat(mus), torch.cat(variances)
```

This yields flattened tensors of all posterior means and variances across the network.

Given two BNNs with posterior parameters (μ_1, σ_1^2) and (μ_2, σ_2^2) , the KL divergence is computed in closed form under the factorized Gaussian assumption:

$$D_{\text{KL}}(p_2\|p_1) = \sum_{i=1}^d \left[\log \frac{\sigma_{1,i}}{\sigma_{2,i}} + \frac{\sigma_{2,i}^2 + (\mu_{2,i} - \mu_{1,i})^2}{2\sigma_{1,i}^2} - \frac{1}{2} \right].$$

We implement the closed-form expression in terms of variances instead of standard deviation with the formula:

```
def gaussian_diagonal_kl(mu_q, var_q, mu_p, var_p):
    return 0.5 * torch.sum(
        torch.log(var_p / var_q)
        + (var_q + (mu_q - mu_p).pow(2)) / var_p - 1)
```

We compute $D_{\text{KL}}(p_2(\omega|\cdot)||p_1(\omega|\cdot))$ after each model change, where $p_1(\omega|\cdot)$ is the previous model posterior and $p_2(\omega|\cdot)$ is the updated posterior. This value is then used in the bounds of Theorems 1 and 2 to assess the robustness of counterfactuals. In practice, this is an approximation as we use BNN's in our robustness experiments to approximate the true posterior parametric distributions, that is our d model weights have parameters for the mean and variance learned approximate parametric posteriors. We note that, experiments in this paper regarding KL divergence between posteriors is calculated only for BNNs.

F ADDITIONAL EXPERIMENTS

F.1 Supplementary δ -Safe Example

To supplement the introduction of the main paper and the first challenge, we consider the following example:

Example 2. *Given an image from the MNIST dataset (LeCun et al., 1998; Deng, 2012) where a model predicts the digit $y = 9$. We aim to find a counterfactual classified as $y' = 8$ with high posterior confidence and bounded variance. Figures 7 and 8 show the counterfactual generation path and the distribution of predictive probabilities on stochastic model samples. The result satisfies the δ -safe and ϵ -robust conditions, offering a plausible and reliable counterfactual.*

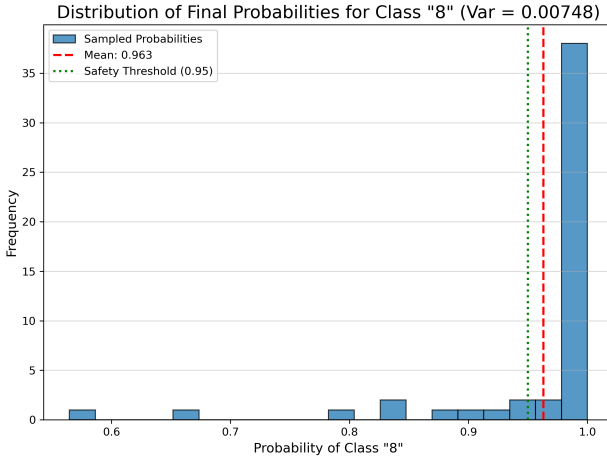


Figure 7: δ -safe and ϵ -robust counterfactual produced by PSCE ($\delta = 0.05$, $\epsilon = 0.01$).

F.2 Complete Ablation

In this section, we show the ablation of different hyper-parameters and the associated image generated under each condition. Thus, in Figure 9a we see the baseline image where all hyperparameters are active in the counterfactual instance generation process. Then, in Figure 9b we remove the term encouraging δ -safety; in Figure 9c we remove the cross-entropy term that encourages the counterfactual instance to reside in the counterfactual class; Figure 9d removes the ELBO term; Figure 9e removes the latent distance term, and thus discouraging proximity in the latent space for the generated counterfactual instance; Figure 9f removes the term encouraging ϵ -robustness.

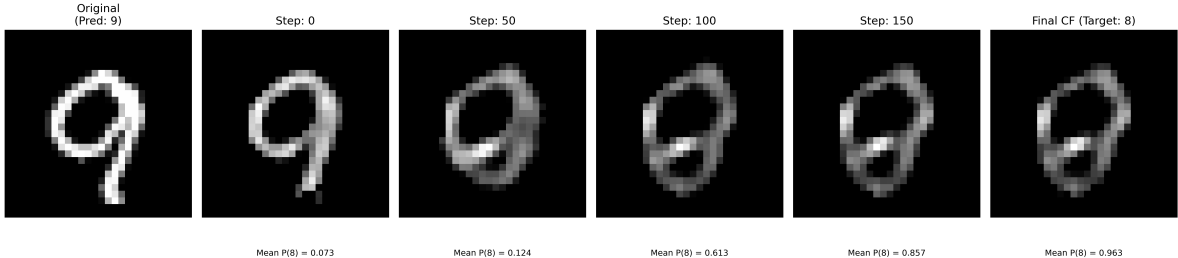


Figure 8: Counterfactual generation process on the MNIST dataset using the proposed PSCE.

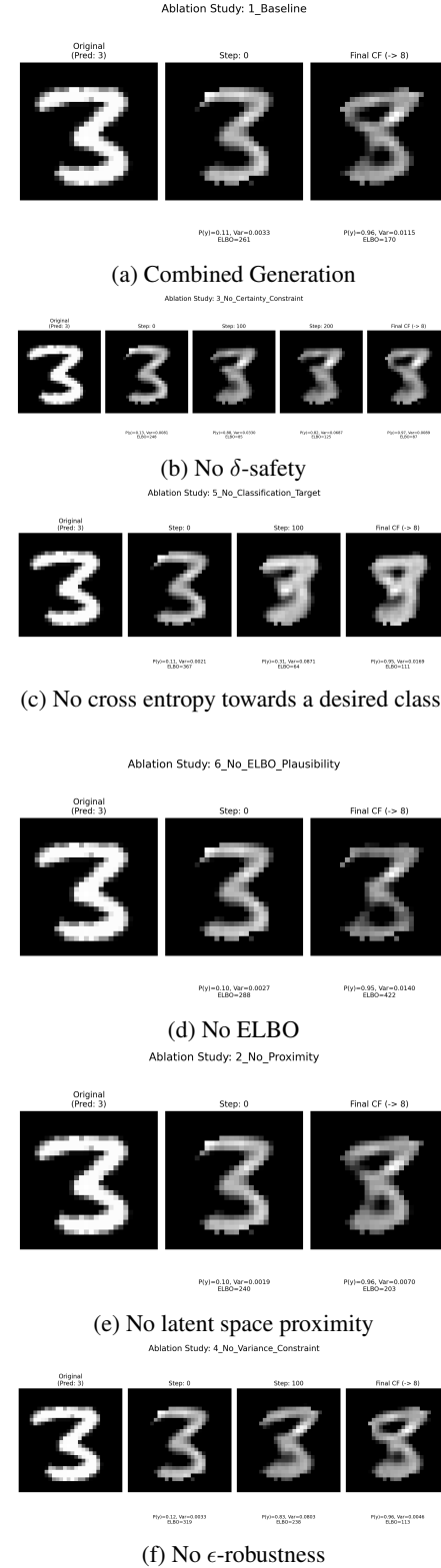


Figure 9: Visual effects of hyperparameter ablation.

G GENERAL DETAILS

G.1 Model Performance Across Seeds

In Table 5, we provide details on the model accuracy across each of the 5 seeds on the 4 datasets experimented in the main manuscript. By which, each of these seeds the counterfactual explanation methods were deployed over 50 instances from the test dataset for each dataset.

Table 4: Model accuracy for each seed the experiments are run on. Since **MC Dropout** in the context of our work, only utilises dropout at inference time for counterfactual instance generation, we record the baseline model performance without dropout enabled.

Dataset	Seed	Accuracy (%)
Breast Cancer	1	96.49
	2	95.61
	3	95.61
	4	95.61
	5	95.61
Credit	1	87.50
	2	79.50
	3	79.00
	4	78.50
	5	79.00
MNIST	1	99.18
	2	99.01
	3	99.07
	4	99.04
	5	99.19
Spam	1	93.92
	2	94.25
	3	94.14
	4	94.03
	5	93.59
PneumoniaMNIST	1	83.33
	2	82.53
	3	85.10
	4	87.02
	5	85.26

G.2 Hyperparameter configuration for Counterfactual methods on each dataset

The hyperparameters were selected subject to performance on the BNN. Each methods hyperparameters were selected based on the validity of counterfactuals.

G.3 Model Architectures

For the implementation of each network, for the MC Dropout-based approaches, VAE and AE we use PyTorch². For the BNN approach we use the bnntorch³ Lee et al. (2022) library. Each network is optimised using the Adaptive Moment Estimation (ADAM) (Kingma and Ba, 2014) optimiser. We use the Log-Softmax activation function for classification and optimize the Negative Log Likelihood (NLL).

²<https://pytorch.org/>

³<https://pypi.org/project/torchbnn/>

Table 5: Model accuracy for each seed the experiments are run on for the **BNN**.

Dataset	Seed	Accuracy (%)
Breast Cancer	1	96.49
	2	95.61
	3	95.61
	4	95.61
	5	95.61
Credit	1	79.00
	2	78.50
	3	77.50
	4	78.50
	5	77.00
MNIST	1	99.11
	2	99.14
	3	98.98
	4	99.10
	5	99.17
Spam	1	93.81
	2	93.70
	3	94.03
	4	93.27
	5	93.49
PneumoniaMNIST	1	84.78
	2	84.46
	3	85.58
	4	84.62
	5	84.78

Table 6: Hyperparameters for Counterfactual Generation Methods for the Spambase and Credit datasets.

Method	Hyperparameter	Description	Value
PSCE	Optimizer	Optimization algorithm	Adam
	Learning Rate	Step size for the optimizer	0.1
	Max Iterations	Maximum optimization steps	2000
	Proximity Weight (λ_{prox})	Weight for the latent space distance loss	0.001
	ELBO Weight (λ_{ELBO})	Weight for the VAE's ELBO loss	0.002
	Classification Weight (λ_{class})	Weight for the negative log probability loss	1.0
	Target Probability (δ)	Minimum required probability for the target class	≥ 0.95
BayesCF	Variance Threshold (ϵ)	Maximum allowed variance in predictions	≤ 0.01
	Optimizer	Optimization algorithm	Adam
	Learning Rate	Step size for the optimizer	0.1
	Max Iterations	Maximum optimization steps	2000
Schut	Proximity Weight (λ_{prox})	Weight for the L2 distance loss in input space	0.001
	Max Iterations	Maximum number of feature perturbations	2000
	Step Size	Magnitude of change for a perturbed feature	0.1
	Max Feature Changes	Maximum times a single feature can be changed	20
	Confidence Threshold	Minimum required confidence for the target class	≥ 0.95

Table 7: Hyperparameters for Counterfactual Generation Methods on the Wisconsin Breast Cancer Dataset.

Method	Hyperparameter	Description	Value
PSCE	Optimizer	Optimization algorithm	Adam
	Learning Rate	Step size for the optimizer	0.1
	Max Iterations	Maximum optimization steps	2000
	Proximity Weight (λ_{prox})	Weight for the latent space distance loss	0.2
	ELBO Weight (λ_{ELBO})	Weight for the VAE's ELBO loss	0.1
	Target Prob. Weight (λ_δ)	Weight for the target probability constraint loss	0.2
	Variance Weight (λ_ϵ)	Weight for the variance constraint loss	0.1
	Classification Weight (λ_{class})	Weight for the negative log likelihood loss	0.1
	Target Probability (δ)	Required confidence for the target class	≥ 0.95
BayesCF	Variance Threshold (ϵ)	Ideal variance in predictions	≤ 0.01
	Optimizer	Optimization algorithm	Adam
	Learning Rate	Step size for the optimizer	0.1
	Max Iterations	Maximum optimization steps	2000
Schut	Proximity Weight (λ_{prox})	Weight for the L2 distance loss in input space	0.1
	Max Iterations	Maximum number of feature perturbations	2000
	Step Size	Magnitude of change for a perturbed feature	0.1
	Max Feature Changes	Maximum times a single feature can be changed	10
Schut	Confidence Threshold	Ideal confidence for the target class	≥ 0.95

Table 8: Hyperparameters for Counterfactual Generation Methods on the MNIST Dataset.

Method	Hyperparameter	Description	Value
PSCE	Optimizer	Optimization algorithm	Adam
	Learning Rate	Step size for the optimizer	0.1
	Max Iterations	Maximum optimization steps	2000
	Proximity Weight (λ_{prox})	Weight for the latent space distance loss	0.0001
	ELBO Weight (λ_{ELBO})	Weight for the VAE's ELBO loss	0.0001
	Target Prob. Weight (λ_δ)	Weight for the target probability constraint loss	1.0
	Variance Weight (λ_ϵ)	Weight for the variance constraint loss	0.1
	Classification Weight (λ_{class})	Weight for the negative log likelihood loss	1.0
	Target Probability (δ)	Required confidence for the target class	≥ 0.95
BayesCF	Variance Threshold (ϵ)	Ideal variance in predictions	≤ 0.01
	Optimizer	Optimization algorithm	Adam
	Learning Rate	Step size for the optimizer	0.1
	Max Iterations	Maximum optimization steps	2000
Schut	Proximity Weight (λ_{prox})	Weight for the L2 distance loss in input space	0.0000001
	Max Iterations	Maximum number of feature perturbations	2000
	Step Size	Magnitude of change for a perturbed feature	0.2
	Max Feature Changes	Maximum times a single feature can be changed	5
Schut	Confidence Threshold	Ideal confidence for the target class	≥ 0.95

Table 9: Architecture of the MC Dropout on the Spambase, Credit and Wisconsin Breast Cancer datasets.

Layer	Type	Configuration	Activation
Input	-	Size: D_{in}	-
1	Fully Connected	$D_{in} \rightarrow 64$	ReLU
2	Dropout	$p = 0.5$	-
3	Fully Connected	$64 \rightarrow 32$	ReLU
4	Dropout	$p = 0.5$	-
5	Fully Connected	$32 \rightarrow C$	Log-Softmax

Table 10: Architecture of the BNN Classifier with Bayesian Layers on the Spambase, Credit and Wisconsin Breast Cancer datasets.

Layer	Type	Configuration	Activation
Input	-	Size: D_{in}	-
1	Bayesian Linear	$D_{in} \rightarrow 64$	ReLU
2	Bayesian Linear	$64 \rightarrow 32$	ReLU
3	Bayesian Linear	$32 \rightarrow C$	Log-Softmax

Table 11: Architecture of the Variational Autoencoder (VAE) on the Spambase, Credit and Wisconsin Breast Cancer datasets.

Component / Layer	Type	Configuration	Activation
<i>Encoder</i>			
Input	-	Size: D_{in}	-
Encoder FC1	Fully Connected	$D_{in} \rightarrow 40$	ReLU
Mean (μ)	Fully Connected	$40 \rightarrow D_z$	Linear
Log-Variance ($\log \sigma^2$)	Fully Connected	$40 \rightarrow D_z$	Linear
<i>Decoder</i>			
Input (Latent)	Reparameterized z	Size: D_z	-
Decoder FC1	Fully Connected	$D_z \rightarrow 40$	ReLU
Output	Fully Connected	$40 \rightarrow D_{in}$	Linear

Table 12: Architecture of the Autoencoder (AE) for the IM1 metric on the Spambase, Credit and Wisconsin Breast Cancer datasets.

Component / Layer	Type	Configuration	Activation
<i>Encoder</i>			
Input	-	Size: D_{in}	-
Encoder FC1	Fully Connected	$D_{in} \rightarrow 40$	ReLU
Encoder FC2	Fully Connected	$40 \rightarrow D_z$	ReLU
<i>Decoder</i>			
Input (Latent)	Encoded Vector	Size: D_z	-
Decoder FC1	Fully Connected	$D_z \rightarrow 40$	ReLU
Output	Fully Connected	$40 \rightarrow D_{in}$	Linear

H Metrics for CE Evaluation

H.1 IM1

The IM1 metric (Van Looveren and Klaise, 2021; Schut et al., 2021), evaluates the ratio of the reconstruction loss with respect to an autoencoder trained on the counterfactual class y' and the reconstruction loss of a counterfactual with an autoencoder (AE) trained on the original class y . Let AE_y be the autoencoder trained on the original class, and $\text{AE}_{y'}$ be the autoencoder trained on the counterfactual class. Then, we have:

$$\text{IM1}(\mathbf{x}') = \frac{\|\mathbf{x}' - \text{AE}_{y'}(\mathbf{x}')\|_2^2}{\|\mathbf{x}' - \text{AE}_y(\mathbf{x}')\|_2^2}.$$

Table 13: Architecture of the CNN Classifier for MNIST used for MC Dropout.

Layer	Type	Configuration	Layer Output Shape
Input	-	-	(1, 28, 28)
Conv-1	Conv2D	10 filters, kernel=5	(10, 24, 24)
Pool-1	Max Pooling	kernel=2, stride=2	(10, 12, 12)
<i>Activation: ReLU</i>			
Conv-2	Conv2D	20 filters, kernel=5	(20, 8, 8)
Drop-2	Dropout2D	p=0.5 (default)	(20, 8, 8)
Pool-2	Max Pooling	kernel=2, stride=2	(20, 4, 4)
<i>Activation: ReLU</i>			
Flatten	Flatten	-	(320)
FC-1	Fully Connected	320 → 50	(50)
<i>Activation: ReLU</i>			
Drop-3	Dropout	p=0.5 (default)	(50)
FC-2 (Output)	Fully Connected	50 → 10	(10)
<i>Activation: Log-Softmax</i>			

Table 14: Architecture of the Variational Autoencoder (VAE) for the MNIST datasets.

Component / Layer	Type	Configuration	Activation
<i>Encoder</i>			
Input	-	Flattened Image (784)	-
FC1	Fully Connected	784 → 400	ReLU
Mean (μ)	Fully Connected	400 → 20	Linear
Log-Var ($\log \sigma^2$)	Fully Connected	400 → 20	Linear
<i>Decoder</i>			
Input (Latent)	Reparameterized z	Size: 20	-
FC3	Fully Connected	20 → 400	ReLU
FC4 (Output)	Fully Connected	400 → 784	ReLU

Table 15: Architecture of the Autoencoder (AE) for the MNIST datasets.

Component / Layer	Type	Configuration	Activation
<i>Encoder</i>			
Input	-	Flattened Image (784)	-
Encoder FC1	Fully Connected	784 → 200	ReLU
Encoder FC2	Fully Connected	200 → 20	ReLU
<i>Decoder</i>			
Input (Latent)	Encoded Vector	Size: 20	-
Decoder FC1	Fully Connected	20 → 200	ReLU
Decoder FC2 (Output)	Fully Connected	200 → 784	Linear

H.2 Robustness Ratio

The robustness ratio adopted in (Batten et al., 2025), explores the robustness of counterfactual explanations subject to a small perturbation in the input instance. More formally:

$$\text{RR}(\mathbf{x}'; \kappa) = \frac{\|\mathcal{G}_{CF}(\mathbf{x} + \kappa) - \mathbf{x}'\|_2^2}{\|\mathbf{x}' - \mathbf{x}\|_2^2}$$

for some $\kappa \ll 1$. We follow implementation details of (Batten et al., 2025) and set $\kappa = 1e - 3$.

Table 16: Architecture of the BNN-CNN with Bayesian Layers for the MNIST datasets.

Layer	Type	Configuration	Layer Output Shape
Input	-	-	(1, 28, 28)
Conv-1	Bayesian Conv2D	10 filters, kernel=5	(10, 24, 24)
Pool-1	Max Pooling	kernel=2, stride=2	(10, 12, 12)
<i>Activation: ReLU</i>			
Conv-2	Bayesian Conv2D	20 filters, kernel=5	(20, 8, 8)
Pool-2	Max Pooling	kernel=2, stride=2	(20, 4, 4)
<i>Activation: ReLU</i>			
Flatten	Flatten	-	(320)
FC-1	Bayesian Linear	320 → 50	(50)
<i>Activation: ReLU</i>			
FC-2 (Output)	Bayesian Linear	50 → 10	(10)
<i>Activation: Log-Sigmoid</i>			



Figure 10: Generated counterfactual examples on a single seed of the BNN.

H.3 Implausibility

Implausibility (Altmeyer et al., 2024) evaluates the mean distance to other instances of the counterfactual class within the training dataset. More formally:

$$\text{Imp}(\mathbf{x}') = \frac{1}{|\mathbf{X}_{y'}|} \sum_{\mathbf{x} \in \mathbf{X}_{y'}} \text{dist}(\mathbf{x}, \mathbf{x}'),$$

where $\mathbf{X}_{y'} \subset \mathbf{X}$ denotes a subset of training data for the target counterfactual class y' , and \mathbf{x}' is a counterfactual instance for $\mathbf{x} \in \mathbf{X}_{y'}$.

H.4 Validity

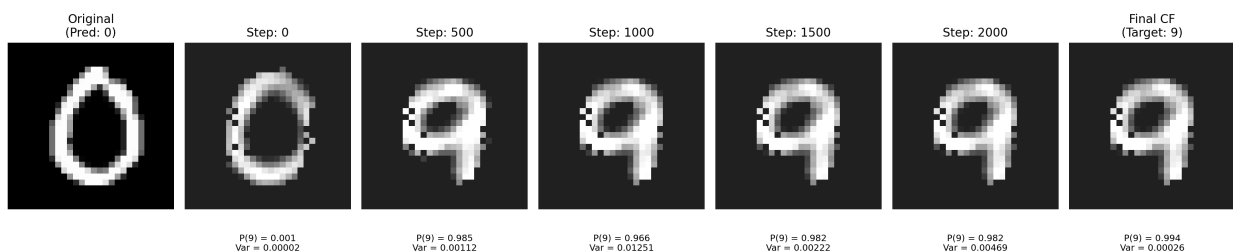
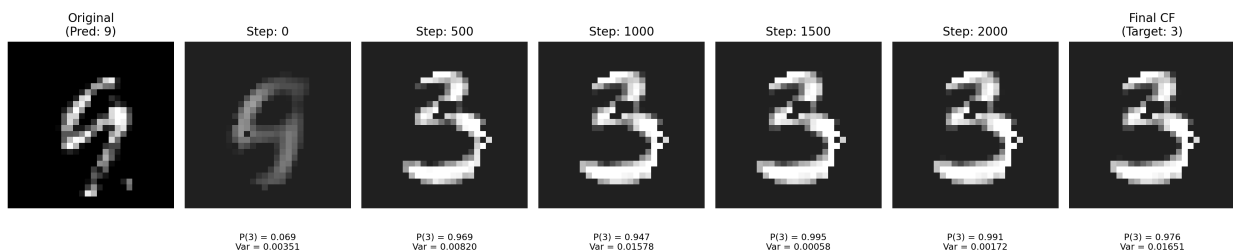
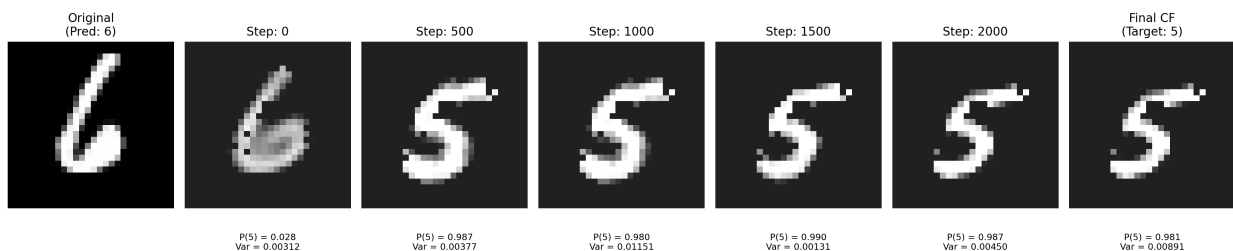
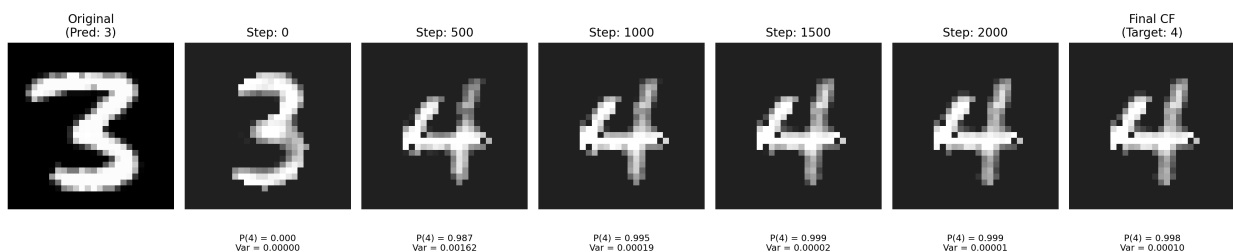
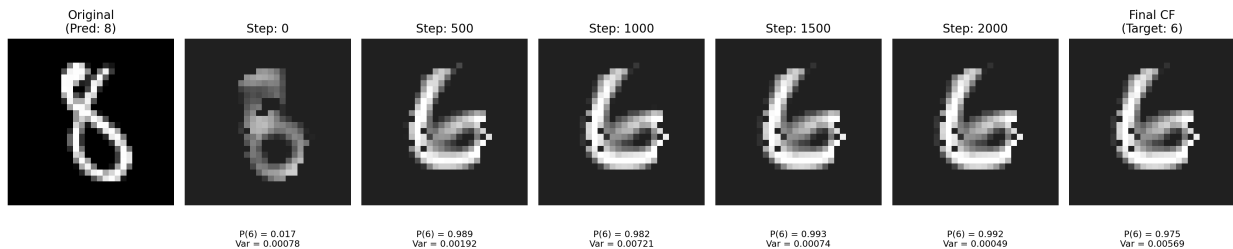
Validity (Mothilal et al., 2020; Batten et al., 2025) looks at the percentage of correctly classified counterfactuals, that is how many counterfactuals belong to the counterfactual class. More formally:

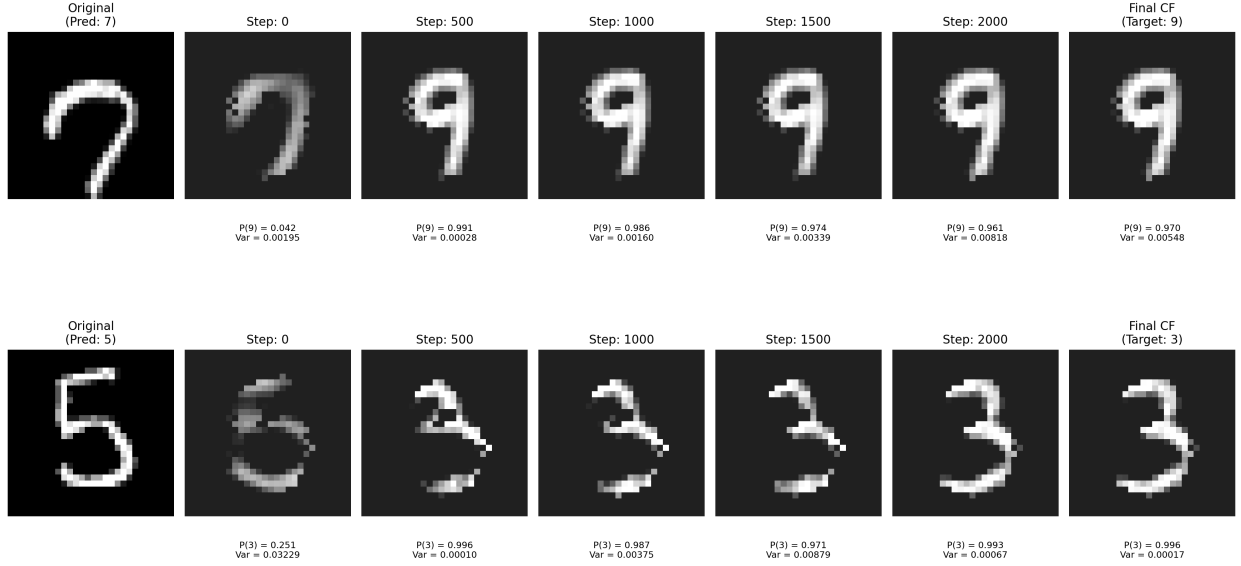
$$\text{Validity}(\mathbf{X}') = \frac{1}{|\mathbf{X}'|} \sum_{\mathbf{x}' \in \mathbf{X}'} \mathbf{1} \left[\arg \max_{c \in \{1, \dots, C\}} p(y = c \mid \mathbf{x}', \mathcal{D}) = y' \right].$$

returning the fraction of counterfactual instances which are correctly classified as y' from the set of generated counterfactuals X' .

I PSCE Examples on MNIST

From Figure 10 we present examples of counterfactuals generated by our method.





J Additional Comparison with Non-Bayesian Baselines

For clarity in the main article we restricted the results including non-Bayesian baselines outlined in Tables 17 and 18, where we consider the Wachter's approach (Wachter et al., 2018) and RObust Algorithmic Recourse (ROAR) (Upadhyay et al., 2021) following their optimisation procedure.

K Limitation and Future work

From a theoretical perspective, an ideal avenue would be to explicitly explore the proposed method empirically under theoretical guarantees in the context of online learning or data drift, as it would present a natural progression for the proposed methodology.

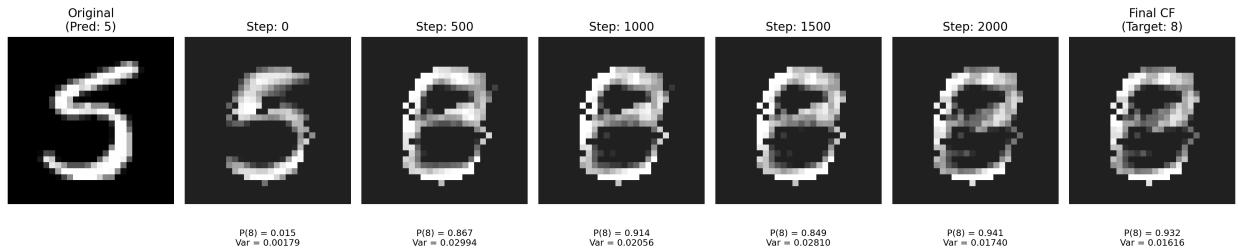


Table 17: Performance metrics measured across all datasets. The best performing method is highlighted in **bold** text. The experiments are run over 5 runs and the *mean* and *standard deviation* are recorded. Each run is evaluated over 100 instances from the test data. These results use **BNN**.

Dataset	Metric	PSCE (Ours)	BayesCF	Schut	Wachter	ROAR
Credit	IM1 (↓)	0.6561 ± 0.0603	0.8311 ± 0.0289	0.9042 ± 0.0222	1.0423 ± 0.0244	1.0285 ± 0.0239
	Implausibility (↓)	8.4606 ± 0.2683	10.1530 ± 0.3799	10.8363 ± 0.1218	9.3963 ± 0.0713	9.3061 ± 0.0677
	Robustness Ratio 1e-3 (↓)	0.1400 ± 0.0203	0.1461 ± 0.0168	0.2318 ± 0.0304	0.5044 ± 0.0176	0.4863 ± 0.0458
	Validity % (↑)	100.0 ± 0.0	100.0 ± 0.0	100.0 ± 0.0	94.4±2.7	95.4±1.0
Breast Cancer	IM1 (↓)	1.5540 ± 0.2427	1.1957 ± 0.0507	1.1151 ± 0.0362	0.8348 ± 0.0251	0.8164 ± 0.0267
	Implausibility (↓)	5.7579 ± 0.0439	7.2014 ± 0.0423	7.4072 ± 0.0333	6.9434 ± 0.0436	6.9247 ± 0.0443
	Robustness Ratio 1e-3 (↓)	0.1566 ± 0.0152	0.3867 ± 0.0306	0.3050 ± 0.0211	0.2684 ± 0.0205	0.2601 ± 0.0214
	Validity % (↑)	86.8±3.2	78.4±3.5	84.8±1.9	99.4±0.5	99.4±0.8
MNIST	IM1 (↓)	0.9768 ± 0.1598	1.6408 ± 0.1267	1.2298 ± 0.0526	1.5153 ± 0.0699	1.4978 ± 0.0739
	Implausibility (↓)	28.1567 ± 0.2665	35.7763 ± 0.0737	31.2247 ± 0.2067	32.1812 ± 0.1574	31.8525 ± 0.1292
	Robustness Ratio 1e-3 (↓)	0.7822 ± 0.0289	1.0191 ± 0.0463	0.9011 ± 0.0170	1.0016 ± 0.0176	0.8750 ± 0.0182
	Validity % (↑)	98.2±1.6	67.6±5.4	96.0±1.8	47.0±5.1	52.8±3.7
Spam	IM1 (↓)	0.7387 ± 0.0578	1.0948 ± 0.0218	0.9137 ± 0.0299	1.1884 ± 0.0173	1.1588 ± 0.0160
	Implausibility (↓)	6.1781 ± 0.0312	9.4032 ± 0.0471	12.9145 ± 0.1061	9.4423 ± 0.0277	9.4445 ± 0.0439
	Robustness Ratio 1e-3 (↓)	0.1028 ± 0.0099	0.1507 ± 0.0124	0.2046 ± 0.0083	0.3883 ± 0.0101	0.3616 ± 0.0106
	Validity % (↑)	96.0 ± 3.3	100.0 ± 0.0	98.6±0.5	97.0±1.1	98.2±0.4
PneumoniaMNIST	IM1 (↓)	0.630 ± 0.095	1.062 ± 0.009	1.157 ± 0.024	1.074 ± 0.013	1.155 ± 0.014
	Implausibility (↓)	4.465 ± 0.332	5.687 ± 0.027	5.350 ± 0.019	5.624 ± 0.021	5.273 ± 0.017
	Robustness Ratio 1e-3 (↓)	0.255 ± 0.020	1.191 ± 0.009	1.015 ± 0.033	1.191 ± 0.017	1.079 ± 0.018
	Validity % (↑)	99.8±0.4	98.4±1.5	91.2±3.6	98.6±0.8	88.0±2.6

Table 18: Performance metrics measured across all datasets. The best performing method is highlighted in **bold** text. The experiments are run over 5 runs and the *mean* and *standard deviation* are recorded. Each run is evaluated over 100 instances from the test data. These results use **MC Dropout**.

Dataset	Metric	PSCE (Ours)	BayesCF	Schut	Wachter	ROAR
Credit	IM1 (↓)	0.7383 ± 0.0341	1.0767 ± 0.0214	0.9251 ± 0.0320	1.0429 ± 0.0236	1.0275 ± 0.0261
	Implausibility (↓)	8.6113 ± 0.1494	9.3615 ± 0.0543	9.9943 ± 0.2124	9.3773 ± 0.0528	9.2826 ± 0.0600
	Robustness Ratio 1e-3 (↓)	0.0622 ± 0.0103	0.1219 ± 0.0106	0.1418 ± 0.0208	0.4867 ± 0.0175	0.4951 ± 0.0304
	Validity % (↑)	100.0±0.0	66.8±5.2	100.0±0.0	95.2±2.2	96.2±1.6
Breast Cancer	IM1 (↓)	0.6932 ± 0.0911	1.1300 ± 0.0306	1.0332 ± 0.0340	0.8214 ± 0.0288	0.8146 ± 0.0328
	Implausibility (↓)	5.6275 ± 0.0627	7.1505 ± 0.0323	7.2913 ± 0.0354	6.8754 ± 0.0680	6.8794 ± 0.0604
	Robustness Ratio 1e-3 (↓)	0.0800 ± 0.0047	0.0539 ± 0.0104	0.1045 ± 0.0105	0.2757 ± 0.0185	0.2757 ± 0.0241
	Validity % (↑)	97.2±1.6	79.2±5.0	90.4±0.8	99.0±1.3	99.4±0.5
MNIST	IM1 (↓)	0.9273 ± 0.0172	1.6426 ± 0.2774	1.2373 ± 0.0392	1.4984 ± 0.0636	1.4739 ± 0.0617
	Implausibility (↓)	27.0337 ± 0.4335	32.9022 ± 0.2163	31.3665 ± 0.1397	31.8151 ± 0.3558	31.5127 ± 0.3418
	Robustness Ratio 1e-3 (↓)	0.6493 ± 0.0496	0.9918 ± 0.0471	1.0696 ± 0.0412	1.0421 ± 0.0324	0.8721 ± 0.0297
	Validity % (↑)	99.6±0.8	47.8±3.3	100.0 ± 0.0	61.6±4.5	75.2±5.2
Spam	IM1 (↓)	0.8967 ± 0.0316	1.4798 ± 0.0122	1.2756 ± 0.0225	1.1112 ± 0.0718	1.0926 ± 0.0686
	Implausibility (↓)	7.2057 ± 0.0618	9.4627 ± 0.0442	10.0120 ± 0.0461	9.4063 ± 0.0565	9.3678 ± 0.0992
	Robustness Ratio 1e-3 (↓)	0.0429 ± 0.0063	0.0868 ± 0.0092	0.0870 ± 0.0151	0.4330 ± 0.0559	0.4356 ± 0.0655
	Validity % (↑)	91.8 ± 4.5	79.0±4.0	99.0±0.0	96.8±2.3	97.0±1.6
PneumoniaMNIST	IM1 (↓)	0.545 ± 0.102	1.062 ± 0.012	1.031 ± 0.007	1.131 ± 0.028	1.109 ± 0.026
	Implausibility (↓)	4.489 ± 0.149	5.647 ± 0.037	6.066 ± 0.138	5.272 ± 0.024	5.312 ± 0.030
	Robustness Ratio 1e-3 (↓)	0.098 ± 0.017	0.597 ± 0.030	0.770 ± 0.034	1.299 ± 0.023	1.346 ± 0.030
	Validity % (↑)	99.4±0.5	100.0±0.0	100.0±0.0	98.0±0.6	98.4±1.2